A polytopal method for the Brinkman problem robust in all regimes

Daniele Antonio Di Pietro, Jérôme Droniou

▶ **To cite this version:**

Daniele Antonio Di Pietro, Jérôme Droniou. A polytopal method for the Brinkman problem robust in all regimes. Computer Methods in Applied Mechanics and Engineering, 2023, 409, pp.115981. 10.1016/j.cma.2023.115981 . hal-03930849

HAL Id: hal-03930849
https://hal.science/hal-03930849v1

Submitted on 9 Jan 2023

HAL is a multi-disciplinary open access archive for the deposit and dissemination of scientific research documents, whether they are published or not. The documents may come from teaching and research institutions in France or abroad, or from public or private research centers.

L'archive ouverte pluridisciplinaire **HAL**, est destinée au dépôt et à la diffusion de documents scientifiques de niveau recherche, publiés ou non, émanant des établissements d'enseignement et de recherche français ou étrangers, des laboratoires publics ou privés.

A polytopal method for the Brinkman problem robust in all regimes

Daniele A. Di Pietro[1] and Jérôme Droniou[2]

[1]IMAG, Univ Montpellier, CNRS, Montpellier, France, daniele.di-pietro@umontpellier.fr
[2]School of Mathematics, Monash University, Melbourne, Australia, jerome.droniou@monash.edu

January 9, 2023

Abstract

In this work we develop a discretisation method for the Brinkman problem that is uniformly well-behaved in all regimes (as identified by a local dimensionless number with the meaning of a friction coefficient) and supports general meshes as well as arbitrary approximation orders. The method is obtained combining ideas from the Hybrid High-Order and Discrete de Rham methods, and its robustness rests on a potential reconstruction and stabilisation terms that change in nature according to the value of the local friction coefficient. We derive error estimates that, thanks to the presence of cut-off factors, are valid across the all regimes and provide extensive numerical validation.

MSC: 65N30, 65N08, 76S05, 76D07

Key words: Brinkman, Darcy, Stokes, Hybrid High-Order methods, Discrete de Rham methods

1 Introduction

The Brinkman problem governs the flow of a viscous fluid in an inhomogeneous material where fractures, bubbles, or channels are present within a porous matrix. Mathematically, this problem translates into a system of partial differential equations with saddle-point structure which can be regarded as a superposition of the Stokes and Darcy systems. As pointed out in [30], the construction of finite element approximations that are uniformly well-behaved across the entire range of (Stokes- or Darcy-dominated) regimes is not straightforward; a representative, but by far not exhaustive, list of references is [2, 4, 12–14, 26, 28, 29, 34]. In [10], we introduced a numerical method for the Brinkman problem on matching simplicial meshes and derived what appears to be the first error estimate accounting for the local regime through a dimensionless number which can be interpreted as a friction coefficient. Thanks to the presence of cutoff factors, this error estimate holds in all situations, including the Stokes problem as well as the singular limit corresponding to the pure Darcy problem.

In this work, we provide a positive answer to an open question left in the above reference, namely whether similar robustness features and error estimates can be obtained on general polytopal meshes. As for the original method of [10], the discretisation of the Stokes term is

inspired by Hybrid High-Order (HHO) methods [19, 21, 23] while, for the Darcy and forcing terms, a novel construction inspired by discrete de Rham methods [17, 20] (see also [22] for an antecedent) replaces the one based on the Raviart–Thomas–Nédélec space [31, 32]. The first central element in this construction is a discrete vector potential that changes in nature depending on the value of the local friction coefficient. The other key ingredient are regime-dependent stabilisation terms. Thanks to these novel tools, we are able to derive a robust estimate of the adjoint error for the discrete divergence, which is the pivot result for the extension of the techniques of [10] to polytopal meshes. The resulting error estimate, stated in Theorem 7 below, is valid on the entire range of values for the local friction coefficient, from 0 (pure Stokes) to $+\infty$ (pure Darcy).

The rest of the work is organised as follows. In Section 2 we briefly recall the continuous and discrete settings. In Section 3 we formulate the numerical scheme and state the main stability and convergence results. Extensive numerical validation of these results on a variety of meshes and regimes for analytical solutions is provided in Section 4, where a more physical three-dimensional test case is also considered. Finally, the proofs of the main results are collected in Section 5.

2 Setting

2.1 Continuous problem

Let $\Omega \subset \mathbb{R}^d$, $d \in \{2,3\}$, denote a bounded connected open polytopal (i.e., polygonal if $d = 2$ and polyhedral if $d = 3$) domain with boundary $\partial\Omega$. For the sake of simplicity, and without loss of generality, we assume that Ω has unit diameter. Let two functions $\mu : \Omega \to \mathbb{R}$ and $\nu : \Omega \to \mathbb{R}$ be given. In what follows, we assume that there exist real numbers $\underline{\mu}$, $\overline{\mu}$, and $\overline{\nu}$ such that, almost everywhere in Ω,

$$0 < \underline{\mu} \le \mu \le \overline{\mu}, \qquad 0 \le \nu \le \overline{\nu}. \tag{1}$$

Let $\boldsymbol{f} : \Omega \to \mathbb{R}^d$ and $g : \Omega \to \mathbb{R}$ denote volumetric source terms. The Brinkman problem reads: Find the velocity $\boldsymbol{u} : \Omega \to \mathbb{R}^d$ and the pressure $p : \Omega \to \mathbb{R}$ such that

$$-\boldsymbol{\nabla}\cdot(\mu\boldsymbol{\nabla}\boldsymbol{u}) + \nu\boldsymbol{u} + \boldsymbol{\nabla}p = \boldsymbol{f} \qquad \text{in } \Omega, \tag{2a}$$

$$\boldsymbol{\nabla}\cdot\boldsymbol{u} = g \qquad \text{in } \Omega, \tag{2b}$$

$$\boldsymbol{u} = \boldsymbol{0} \qquad \text{on } \partial\Omega, \tag{2c}$$

$$\int_\Omega p = 0. \tag{2d}$$

A few simplifications are made to make the exposition more compact while retaining all the difficulties related to the robustness across the entire range of values for μ and ν. First of all, in (2a) we have considered a viscous term expressed in terms of the full gradient instead of its symmetric part $\boldsymbol{\nabla}_{\mathrm{s}}$. The changes to replace $\boldsymbol{\nabla}$ with $\boldsymbol{\nabla}_{\mathrm{s}}$ are standard in the HHO literature; see, e.g., [11, 21] and [19, Chapter 7]. Second, we assume henceforth that both μ and ν are piecewise constant on a polytopal partition P_Ω of the domain. The extension to coefficients that vary smoothly inside each element, and are possibly full tensors, is also standard; see, in particular, [19, Section 4.2].

2.2 Discrete setting

2.2.1 Mesh and notation for inequalities up to a constant

We consider polytopal meshes $\mathcal{M}_h \coloneqq \mathcal{T}_h \cup \mathcal{F}_h$ matching the geometrical requirements detailed in [19, Definition 1.4], with $\mathcal{T}_h$ set of elements and $\mathcal{F}_h$ set of faces. To avoid dealing with jumps of the problem coefficients μ and ν inside mesh elements, we additionally assume that $\mathcal{T}_h$ is compatible with P_Ω, meaning that, for each $T \in \mathcal{T}_h$, there exists $\omega \in P_\Omega$ such that $T \subset \omega$. We then set $\mu_T \coloneqq \mu_{|T}$ and $\nu_T \coloneqq \nu_{|T}$ for all $T \in \mathcal{T}_h$, noticing that these constant values are uniquely defined in each element. For any $Y \in \mathcal{M}_h$, we denote by h_Y its diameter, so that $h = \max_{T\in\mathcal{T}_h} h_T > 0$. For every mesh element $T \in \mathcal{T}_h$, we denote by $\mathcal{F}_T$ the subset of $\mathcal{F}_h$ containing the faces that lie on the boundary ∂T of T. For any mesh face $F \in \mathcal{F}_h$, we fix once and for all a unit normal vector $\boldsymbol{n}_F$ and, for any mesh element $T \in \mathcal{T}_h$ such that $F \in \mathcal{F}_T$, we let $\omega_{TF} \in \{-1, +1\}$ denote the orientation of F relative to T, selected so that $\omega_{TF}\boldsymbol{n}_F$ points out of T. Boundary faces lying on $\partial\Omega$ are collected in the set $\mathcal{F}_h^{\mathrm{b}}$.

Our focus being on the h-convergence analysis, we assume that $\mathcal{M}_h$ belongs to a sequence of refined polygonal or polyhedral meshes that is regular in the sense of [19, Definition 1.9]. This implies, in particular, that the number of faces of each mesh element is bounded from above by an integer independent of h; see [19, Lemma 1.12].

From this point on, $a \lesssim b$ (resp. $a \gtrsim b$) means $a \le Cb$ (resp. $a \ge Cb$) with C only depending on Ω, the mesh regularity parameter, and the polynomial degree k of the scheme defined in Section 3. We stress that this means, in particular, that C is independent of the problem parameters μ and ν. We also write $a \simeq b$ as a shorthand for "$a \lesssim b$ and $b \lesssim a$".

2.2.2 Polynomial spaces

Given $Y \in \mathcal{T}_h \cup \mathcal{F}_h$ and an integer $m \ge 0$, we denote by $\mathcal{P}^m(Y)$ the space spanned by the restriction to Y of d-variate polynomials of total degree $\le m$. The symbols $\boldsymbol{\mathcal{P}}^m(Y;\mathbb{R}^d)$ and $\boldsymbol{\mathcal{P}}^m(Y;\mathbb{R}^{d\times d})$ respectively denote the sets of vector- and tensor-valued functions over Y whose components are in $\mathcal{P}^m(Y)$. For $T \in \mathcal{T}_h$, we will need the following direct decomposition of $\boldsymbol{\mathcal{P}}^m(T;\mathbb{R}^d)$ (see, e.g., [5, Corollary 7.4]):

$$\boldsymbol{\mathcal{P}}^m(T;\mathbb{R}^d) = \boldsymbol{\mathcal{G}}^m(T) \oplus \boldsymbol{\mathcal{G}}^{\mathrm{c},m}(T),$$

with

$$\boldsymbol{\mathcal{G}}^m(T) \coloneqq \boldsymbol{\nabla}\mathcal{P}^{m+1}(T) \quad \text{and} \quad \boldsymbol{\mathcal{G}}^{\mathrm{c},m}(T) \coloneqq \begin{cases} (\boldsymbol{x}-\boldsymbol{x}_T)^\perp\mathcal{P}^{m-1}(T) & \text{if } d=2,\\ (\boldsymbol{x}-\boldsymbol{x}_T)\times\boldsymbol{\mathcal{P}}^{m-1}(T;\mathbb{R}^3) & \text{if } d=3,\end{cases} \tag{3}$$

where $\boldsymbol{x}_T$ is a point such that T is star-shaped with respect to a ball of radius $\gtrsim h_T$ and, in the case $d = 2$, for any $\boldsymbol{v} \in \mathbb{R}^2$ we denote by $\boldsymbol{v}^\perp$ the vector obtained rotating $\boldsymbol{v}$ by $-\frac{\pi}{2}$ radians. Given a polynomial (sub)space $\mathcal{X}^m(Y)$ on $Y \in \mathcal{T}_h \cup \mathcal{F}_h$, the corresponding L^2-orthogonal projector is denoted by $\pi^m_{\mathcal{X},Y}$. Boldface fonts will be used when the elements of $\mathcal{X}^m(Y)$ are vector-valued. The set of broken polynomials of total degree $\le m$ on the mesh is denoted by $\mathcal{P}^m(\mathcal{T}_h)$, and the corresponding L^2-orthogonal projector by $\pi^m_{\mathcal{P},h}$.

2.2.3 Local friction coefficient

The regime inside each mesh element $T \in \mathcal{T}_h$ is identified by the following dimensionless number, which can be interpreted as a friction coefficient:

$$C_{\mathrm{f},T} \coloneqq \frac{\nu_T h_T^2}{\mu_T}. \tag{4}$$

Elements for which $C_{\mathrm{f},T} < 1$ are in the Stokes-dominated regime, while elements for which $C_{\mathrm{f},T} \geq 1$ are in the Darcy-dominated regime. The values $C_{\mathrm{f},T} = 0$ and $C_{\mathrm{f},T} = +\infty$ correspond to pure Stokes and pure Darcy, respectively. Notice that $C_{\mathrm{f},T} = +\infty$ is a singular limit which, despite requiring to modify the continuous formulation (2), can be handled seamlessly by the method developed in the next section; see Remark 8 below.

3 A robust numerical scheme for the Brinkman problem

3.1 Spaces

Let an integer $k \geq 0$ be fixed. We define the following HHO space:

$$\underline{\boldsymbol{U}}_h^k \coloneqq \Big\{ \underline{\boldsymbol{v}}_h = \big((\boldsymbol{v}_T)_{T\in\mathcal{T}_h}, (\boldsymbol{v}_F)_{F\in\mathcal{F}_h}\big) : \boldsymbol{v}_T \in \boldsymbol{\mathcal{P}}^k(T;\mathbb{R}^d) \text{ for all } T \in \mathcal{T}_h \text{ and } \boldsymbol{v}_F \in \boldsymbol{\mathcal{P}}^k(F;\mathbb{R}^d) \text{ for all } F \in \mathcal{F}_h \Big\}.$$

The meaning of the polynomial components in $\underline{\boldsymbol{U}}_h^k$ is provided by the interpolator $\underline{\boldsymbol{I}}_h^k : \boldsymbol{H}^1(\Omega;\mathbb{R}^d) \to \underline{\boldsymbol{U}}_h^k$ such that, for all $\boldsymbol{v} \in \boldsymbol{H}^1(\Omega;\mathbb{R}^d)$,

$$\underline{\boldsymbol{I}}_h^k \boldsymbol{v} \coloneqq \big((\boldsymbol{\pi}_{\boldsymbol{\mathcal{P}},T}^k \boldsymbol{v})_{T\in\mathcal{T}_h}, (\boldsymbol{\pi}_{\boldsymbol{\mathcal{P}},F}^k \boldsymbol{v})_{F\in\mathcal{T}_h},\big) \in \underline{\boldsymbol{U}}_h^k,$$

where it is understood that L^2-orthogonal projectors are applied to restrictions or traces as needed. The restrictions of $\underline{\boldsymbol{U}}_h^k$, $\underline{\boldsymbol{v}}_h \in \underline{\boldsymbol{U}}_h^k$, and $\underline{\boldsymbol{I}}_h^k$ to a mesh element T, respectively denoted by $\underline{\boldsymbol{U}}_T^k$, $\underline{\boldsymbol{v}}_T \in \underline{\boldsymbol{U}}_T^k$, and $\underline{\boldsymbol{I}}_T^k$, are obtained collecting the components attached to T and its faces.

In what follows, given a logical proposition P, we denote by $\langle P\rangle$ its truth value such that

$$\langle P\rangle \coloneqq \begin{cases} 0 & \text{if } P \text{ is false,} \\ 1 & \text{if } P \text{ is true.} \end{cases} \tag{5}$$

We define the following L^2-like product in $\underline{\boldsymbol{U}}_h^k$: For all $(\underline{\boldsymbol{w}}_h, \underline{\boldsymbol{v}}_h) \in \underline{\boldsymbol{U}}_h^k \times \underline{\boldsymbol{U}}_h^k$,

$$\begin{aligned} (\underline{\boldsymbol{w}}_h, \underline{\boldsymbol{v}}_h)_{U,h} &\coloneqq \sum_{T\in\mathcal{T}_h} (\underline{\boldsymbol{w}}_T, \underline{\boldsymbol{v}}_T)_{U,T} \quad \text{with} \\ (\underline{\boldsymbol{w}}_T, \underline{\boldsymbol{v}}_T)_{U,T} &\coloneqq \lambda_T \int_T \boldsymbol{w}_T \cdot \boldsymbol{v}_T + h_T \sum_{F\in\mathcal{F}_T} \langle C_{\mathrm{f},T} < 1 \text{ or } F \notin \mathcal{F}_h^{\mathrm{b}}\rangle \int_F \boldsymbol{w}_F \cdot \boldsymbol{v}_F, \end{aligned} \tag{6}$$

where $\lambda_T \simeq 1$ is a factor, based on the regularity of the element T, chosen to balance out the element and face contributions to $(\cdot,\cdot)_{U,T}$ (see Section 4). The corresponding local and global seminorms are obtained setting, for $\bullet \in \mathcal{T}_h \cup \{h\}$,

$$\|\underline{\boldsymbol{v}}_\bullet\|_{U,\bullet} \coloneqq (\underline{\boldsymbol{v}}_\bullet, \underline{\boldsymbol{v}}_\bullet)_{U,\bullet}^{1/2}. \tag{7}$$

The following boundedness property of the interpolator in the $\|\cdot\|_{\underline{U},h}$-norm follows from the definition of this norm along with the uniform boundedness of the L^2-orthogonal projectors $\boldsymbol{\pi}^k_{\boldsymbol{\mathcal{P}},Y}$, $Y \in \mathcal{M}_h$, and continuous trace inequalities (cf. [19, Lemma 1.31]): For all $T \in \mathcal{T}_h$ and all $\boldsymbol{v} \in \boldsymbol{H}^1(T;\mathbb{R}^d)$,

$$\|\underline{\boldsymbol{I}}^k_T \boldsymbol{v}\|_{\underline{U},T} \lesssim \|\boldsymbol{v}\|_{\boldsymbol{L}^2(T;\mathbb{R}^d)} + h_T|\boldsymbol{v}|_{\boldsymbol{H}^1(T;\mathbb{R}^d)}. \tag{8}$$

The velocity and pressure spaces, respectively incorporating the boundary and zero-average conditions, are

$$\underline{\boldsymbol{U}}^k_{h,0} \coloneqq \left\{ \underline{\boldsymbol{v}}_h \in \underline{\boldsymbol{U}}^k_h \ : \ \boldsymbol{v}_F = \boldsymbol{0} \text{ for all } F \in \mathcal{F}^{\mathrm{b}}_h \right\}, \qquad P^k_h \coloneqq \mathcal{P}^k(\mathcal{T}_h) \cap L^2_0(\Omega),$$

where, as usual, $L^2_0(\Omega) = \left\{ q \in L^2(\Omega) \ : \ \int_\Omega q = 0 \right\}$.

Remark 1 (Boundary degrees of freedom). Note that the degrees of freedom on the boundary faces of a vector in $\underline{\boldsymbol{U}}^k_h$ may not be controlled by the seminorms $\|\cdot\|_{\underline{U},\bullet}$. This is, however, not an issue as the final problem will be set on $\underline{\boldsymbol{U}}^k_{h,0}$ (see also Remark 8 for the handling of boundary values in the limiting case of the pure Darcy problem).

3.2 Viscous term

Let $T \in \mathcal{T}_h$ be fixed. For the discretisation of the viscous term, we define the *discrete gradient* $\boldsymbol{G}^k_T : \underline{\boldsymbol{U}}^k_T \to \boldsymbol{\mathcal{P}}^k(T;\mathbb{R}^{d\times d})$ and the *Stokes potential* $\boldsymbol{P}^{k+1}_{\mathrm{S},T} : \underline{\boldsymbol{U}}^k_T \to \boldsymbol{\mathcal{P}}^k(T;\mathbb{R}^d)$ such that, for all $\underline{\boldsymbol{v}}_T \in \underline{\boldsymbol{U}}^k_T$,

$$\int_T \boldsymbol{G}^k_T \underline{\boldsymbol{v}}_T : \boldsymbol{\tau} = -\int_T \boldsymbol{v}_T \cdot \boldsymbol{\nabla}\cdot\boldsymbol{\tau} + \sum_{F\in\mathcal{F}_T} \omega_{TF} \int_F \boldsymbol{v}_F \cdot \boldsymbol{\tau}\boldsymbol{n}_F \qquad \forall \boldsymbol{\tau} \in \boldsymbol{\mathcal{P}}^k(T;\mathbb{R}^{d\times d}), \tag{9}$$

and

$$\boldsymbol{\nabla}\boldsymbol{P}^{k+1}_{\mathrm{S},T}\underline{\boldsymbol{v}}_T = \boldsymbol{\pi}^k_{\boldsymbol{\mathcal{G}},T}\boldsymbol{G}^k_T\underline{\boldsymbol{v}}_T, \qquad \int_T \boldsymbol{P}^{k+1}_{\mathrm{S},T}\underline{\boldsymbol{v}}_T = \int_T \boldsymbol{v}_T, \tag{10}$$

with $\boldsymbol{\pi}^k_{\boldsymbol{\mathcal{G}},T}$ applied to tensor-valued fields also acting row-wise. Likewise, in the formulas above, $\boldsymbol{\nabla}\cdot$ and $\boldsymbol{\nabla}$ are understood to act row-wise.

The Stokes term in (2a) is discretised through the bilinear form $a_{\mu,h} : \underline{\boldsymbol{U}}^k_h \times \underline{\boldsymbol{U}}^k_h \to \mathbb{R}$ such that, for all $(\underline{\boldsymbol{w}}_h, \underline{\boldsymbol{v}}_h) \in \underline{\boldsymbol{U}}^k_h \times \underline{\boldsymbol{U}}^k_h$,

$$a_{\mu,h}(\underline{\boldsymbol{w}}_h, \underline{\boldsymbol{v}}_h) \coloneqq \sum_{T\in\mathcal{T}_h} \mu_T a_{\mathrm{S},T}(\underline{\boldsymbol{w}}_T, \underline{\boldsymbol{v}}_T), \tag{11}$$

where, for all $T \in \mathcal{T}_h$,

$$a_{\mathrm{S},T}(\underline{\boldsymbol{w}}_T, \underline{\boldsymbol{v}}_T) \coloneqq \int_T \boldsymbol{G}^k_T\underline{\boldsymbol{w}}_T : \boldsymbol{G}^k_T\underline{\boldsymbol{v}}_T + \frac{\min(1, C^{-1}_{\mathrm{f},T})}{h^2_T}(\underline{\boldsymbol{w}}_T - \underline{\boldsymbol{I}}^k_T\boldsymbol{P}^{k+1}_{\mathrm{S},T}\underline{\boldsymbol{w}}_T, \underline{\boldsymbol{v}}_T - \underline{\boldsymbol{I}}^k_T\boldsymbol{P}^{k+1}_{\mathrm{S},T}\underline{\boldsymbol{v}}_T)_{\underline{U},T}. \tag{12}$$

We define the following induced seminorms: For all $\underline{\boldsymbol{v}}_h \in \underline{\boldsymbol{U}}^k_h$,

$$\|\underline{\boldsymbol{v}}_h\|_{\mu,h} \coloneqq a_{\mu,h}(\underline{\boldsymbol{v}}_h, \underline{\boldsymbol{v}}_h)^{1/2} \quad \text{and} \quad \|\underline{\boldsymbol{v}}_T\|_{\mathrm{S},T} \coloneqq a_{\mathrm{S},T}(\underline{\boldsymbol{v}}_T, \underline{\boldsymbol{v}}_T)^{1/2} \text{ for all } T \in \mathcal{T}_h. \tag{13}$$

Lemma 2 (Norm equivalence). *Let $T \in \mathcal{T}_h$ and $\underline{\boldsymbol{v}}_T \in \underline{\boldsymbol{U}}_T^k$. Then, it holds*

$$\|\boldsymbol{\nabla} \boldsymbol{v}_T\|_{\boldsymbol{L}^2(T;\mathbb{R}^{d\times d})}^2 + \frac{1}{h_T} \sum_{F\in\mathcal{F}_T} \|\boldsymbol{v}_T - \boldsymbol{v}_F\|_{\boldsymbol{L}^2(F;\mathbb{R}^d)}^2 \gtrsim \|\underline{\boldsymbol{v}}_T\|_{\mathrm{S},T}^2. \tag{14}$$

Assuming, moreover, $C_{\mathrm{f},T} < 1$, we also have

$$\|\boldsymbol{\nabla} \boldsymbol{v}_T\|_{\boldsymbol{L}^2(T;\mathbb{R}^{d\times d})}^2 + \frac{1}{h_T} \sum_{F\in\mathcal{F}_T} \|\boldsymbol{v}_T - \boldsymbol{v}_F\|_{\boldsymbol{L}^2(F;\mathbb{R}^d)}^2 \lesssim \|\underline{\boldsymbol{v}}_T\|_{\mathrm{S},T}^2. \tag{15}$$

Proof. For the sake of brevity, we only prove (15). The proof of (14) hinges on similar arguments, together with the fact that $\min(1, C_{\mathrm{f},T}^{-1}) \le 1$, and is left to the reader. Taking $\boldsymbol{\tau} = \boldsymbol{\nabla} \boldsymbol{v}_T$ in (9), integrating by parts the first term in the right-hand side, and using Cauchy–Schwarz and discrete trace inequalities (see [19, Lemma 1.32]) as in the proof of [19, Eq. (2.25)], we get, after simplifying and raising to the square,

$$\|\boldsymbol{\nabla} \boldsymbol{v}_T\|_{\boldsymbol{L}^2(T;\mathbb{R}^{d\times d})}^2 \lesssim \|\boldsymbol{G}_T^k \underline{\boldsymbol{v}}_T\|_{\boldsymbol{L}^2(T;\mathbb{R}^{d\times d})}^2 + h_T^{-1} \sum_{F\in\mathcal{F}_T} \|\boldsymbol{v}_T - \boldsymbol{v}_F\|_{\boldsymbol{L}^2(F;\mathbb{R}^d)}^2. \tag{16}$$

To estimate the second term, for any $F \in \mathcal{F}_T$, we insert $\pm(\boldsymbol{\pi}_{\mathcal{P},T}^k \boldsymbol{P}_{\mathrm{S},T}^{k+1} \underline{\boldsymbol{v}}_T - \boldsymbol{\pi}_{\mathcal{P},F}^k \boldsymbol{P}_{\mathrm{S},T}^{k+1} \underline{\boldsymbol{v}}_T)$ and use triangle inequalities to get

$$\begin{aligned}
h_T^{-1}\|\boldsymbol{v}_T - \boldsymbol{v}_F\|_{\boldsymbol{L}^2(F;\mathbb{R}^d)}^2 &\lesssim h_T^{-1}\|\boldsymbol{v}_T - \boldsymbol{\pi}_{\mathcal{P},T}^k \boldsymbol{P}_{\mathrm{S},T}^{k+1} \underline{\boldsymbol{v}}_T\|_{\boldsymbol{L}^2(F;\mathbb{R}^d)}^2 + h_T^{-1}\|\boldsymbol{v}_F - \boldsymbol{\pi}_{\mathcal{P},F}^k \boldsymbol{P}_{\mathrm{S},T}^{k+1} \underline{\boldsymbol{v}}_T\|_{\boldsymbol{L}^2(F;\mathbb{R}^d)}^2 \\
&\quad + h_T^{-1}\|\boldsymbol{\pi}_{\mathcal{P},F}^k (\boldsymbol{P}_{\mathrm{S},T}^{k+1} \underline{\boldsymbol{v}}_T - \boldsymbol{\pi}_{\mathcal{P},T}^k \boldsymbol{P}_{\mathrm{S},T}^{k+1} \underline{\boldsymbol{v}}_T)\|_{\boldsymbol{L}^2(F;\mathbb{R}^d)}^2 \\
&\lesssim h_T^{-2}\|\boldsymbol{v}_T - \boldsymbol{\pi}_{\mathcal{P},T}^k \boldsymbol{P}_{\mathrm{S},T}^{k+1} \underline{\boldsymbol{v}}_T\|_{\boldsymbol{L}^2(T;\mathbb{R}^d)}^2 + h_T^{-1}\|\boldsymbol{v}_F - \boldsymbol{\pi}_{\mathcal{P},F}^k \boldsymbol{P}_{\mathrm{S},T}^{k+1} \underline{\boldsymbol{v}}_T\|_{\boldsymbol{L}^2(F;\mathbb{R}^d)}^2 \\
&\quad + h_T^{-2}\|\boldsymbol{P}_{\mathrm{S},T}^{k+1} \underline{\boldsymbol{v}}_T - \boldsymbol{\pi}_{\mathcal{P},T}^k \boldsymbol{P}_{\mathrm{S},T}^{k+1} \underline{\boldsymbol{v}}_T\|_{\boldsymbol{L}^2(T;\mathbb{R}^d)}^2 \\
&\lesssim h_T^{-2}\|\underline{\boldsymbol{v}}_T - \underline{\boldsymbol{I}}_T^k \boldsymbol{P}_{\mathrm{S},T}^{k+1} \underline{\boldsymbol{v}}_T\|_{U,T}^2 + \|\boldsymbol{\nabla} \boldsymbol{P}_{\mathrm{S},T}^{k+1} \underline{\boldsymbol{v}}_T\|_{\boldsymbol{L}^2(T;\mathbb{R}^{d\times d})}^2 \\
&\lesssim \frac{\min(1, C_{\mathrm{f},T}^{-1})}{h_T^2}\|\underline{\boldsymbol{v}}_T - \underline{\boldsymbol{I}}_T^k \boldsymbol{P}_{\mathrm{S},T}^{k+1} \underline{\boldsymbol{v}}_T\|_{U,T}^2 + \|\boldsymbol{G}_T^k \underline{\boldsymbol{v}}_T\|_{\boldsymbol{L}^2(T;\mathbb{R}^{d\times d})}^2 = \|\underline{\boldsymbol{v}}_T\|_{\mathrm{S},T}^2,
\end{aligned} \tag{17}$$

where we have used the L^2-boundedness of $\boldsymbol{\pi}_{\mathcal{P},F}^k$ along with discrete trace inequalities in the second passage, the definition (7) of $\|\cdot\|_{U,T}$ along with $C_{\mathrm{f},T} < 1$ for the first two terms and the approximation properties of $\boldsymbol{\pi}_{\mathcal{P},T}^k$ for the last term in the third passage, and concluded noticing that $1 = \min(1, C_{\mathrm{f},T}^{-1})$ and that $\boldsymbol{\nabla} \boldsymbol{P}_{\mathrm{S},T}^{k+1} \underline{\boldsymbol{v}}_T$ is by definition the L^2-orthogonal projection of $\boldsymbol{G}_T^k \underline{\boldsymbol{v}}_T$ on $\boldsymbol{\mathcal{G}}^k(T)^d$ (see (10)), so that $\|\boldsymbol{\nabla} \boldsymbol{P}_{\mathrm{S},T}^{k+1} \underline{\boldsymbol{v}}_T\|_{\boldsymbol{L}^2(T;\mathbb{R}^{d\times d})} \le \|\boldsymbol{G}_T^k \underline{\boldsymbol{v}}_T\|_{\boldsymbol{L}^2(T;\mathbb{R}^{d\times d})}$. Plugging (17) into (16) and using the fact that $\mathrm{card}(\mathcal{F}_T) \lesssim 1$ by mesh regularity, we get $\|\boldsymbol{\nabla} \boldsymbol{v}_T\|_{\boldsymbol{L}^2(T;\mathbb{R}^{d\times d})}^2 \lesssim \|\underline{\boldsymbol{v}}_T\|_{\mathrm{S},T}^2$, which is the sought estimate for the first term in the left-hand side of (15). The fact second term is $\lesssim \|\underline{\boldsymbol{v}}_T\|_{\mathrm{S},T}^2$ is an immediate consequence of (17) along with $\mathrm{card}(\mathcal{F}_T) \lesssim 1$. □

Remark 3 (HHO stabilisation). It is not difficult to check that the bilinear form $\underline{\boldsymbol{U}}_T^k \times \underline{\boldsymbol{U}}_T^k \ni (\underline{\boldsymbol{w}}_T, \underline{\boldsymbol{v}}_T) \mapsto (\underline{\boldsymbol{w}}_T - \underline{\boldsymbol{I}}_T^k \boldsymbol{P}_{\mathrm{S},T}^{k+1} \underline{\boldsymbol{w}}_T, \underline{\boldsymbol{v}}_T - \underline{\boldsymbol{I}}_T^k \boldsymbol{P}_{\mathrm{S},T}^{k+1} \underline{\boldsymbol{v}}_T)_{U,T}$ matches [19, Assumption 8.10]. As a matter of fact, this bilinear form is clearly positive-semidefinite, it satisfies the requested seminorm equivalence by (14) and (15), and is polynomially consistent since it only depends on its arguments through the difference operators defined by [19, Eq. (8.30)].

3.3 Darcy term

Let again $T \in \mathcal{T}_h$. The discretisation of the Darcy and coupling terms hinges on the *discrete divergence* $D_T^k : \underline{\boldsymbol{U}}_T^k \to \mathcal{P}^k(T)$ such that

$$D_T^k \underline{\boldsymbol{v}}_T \coloneqq \mathrm{tr}(\boldsymbol{G}_T^k \underline{\boldsymbol{v}}_T) \qquad \forall \underline{\boldsymbol{v}}_T \in \underline{\boldsymbol{U}}_T^k. \tag{18}$$

Based on this operator, we define the *Darcy potential* $\boldsymbol{P}_{\mathrm{D},T}^k : \underline{\boldsymbol{U}}_T^k \to \boldsymbol{\mathcal{P}}^k(T;\mathbb{R}^d)$ such that, for all $\underline{\boldsymbol{v}}_T \in \underline{\boldsymbol{U}}_T^k$ and all $(q, \boldsymbol{w}) \in \mathcal{P}^{k+1}(T) \times \boldsymbol{\mathcal{G}}^{\mathrm{c},k}(T)$,

$$\int_T \boldsymbol{P}_{\mathrm{D},T}^k \underline{\boldsymbol{v}}_T \cdot (\boldsymbol{\nabla} q + \boldsymbol{w}) = -\int_T D_T^k \underline{\boldsymbol{v}}_T \, q + \sum_{F \in \mathcal{F}_T} \omega_{TF} \int_F (\boldsymbol{v}_F \cdot \boldsymbol{n}_F) \, q + \int_T \boldsymbol{v}_T \cdot \boldsymbol{w}. \tag{19}$$

This Darcy potential will play a key role in the discretisation of the source term, to ensure that the scheme is fully robust in the whole range of friction coefficients; see Remark 13.

Remark 4 (Link with DDR). Recall the Discrete De Rham $\boldsymbol{H}(\mathrm{div};\Omega)$-like space

$$\begin{aligned}\underline{\boldsymbol{X}}_{\mathrm{div},h}^k \coloneqq \Big\{ \underline{\boldsymbol{v}}_h = \big((\boldsymbol{v}_{\mathcal{G},T}, \boldsymbol{v}_{\mathcal{G},T}^{\mathrm{c}})_{T\in\mathcal{T}_h}, (v_F)_{F\in\mathcal{F}_h}\big) \ : \\ \boldsymbol{v}_{\mathcal{G},T} \in \boldsymbol{\mathcal{G}}^{k-1}(T) \text{ and } \boldsymbol{v}_{\mathcal{G},T}^{\mathrm{c}} \in \boldsymbol{\mathcal{G}}^{\mathrm{c},k}(T) \text{ for all } T \in \mathcal{T}_h, \\ v_F \in \mathcal{P}^k(F) \text{ for all } F \in \mathcal{F}_h \Big\}.\end{aligned}$$

Noticing that $\boldsymbol{\mathcal{G}}^{k-1}(T) \subset \boldsymbol{\mathcal{G}}^k(T)$ (cf. (3)), this space injects into $\underline{\boldsymbol{U}}_h^k$ through the mapping

$$\underline{\boldsymbol{X}}_{\mathrm{div},h}^k \ni \underline{\boldsymbol{v}}_h \mapsto \big((\mathfrak{R}_{\mathcal{G},T}^k(\boldsymbol{v}_{\mathcal{G},T}, \boldsymbol{v}_{\mathcal{G},T}^{\mathrm{c}}))_{T\in\mathcal{T}_h}, (v_F \boldsymbol{n}_F)_{F\in\mathcal{F}_h}\big) \in \underline{\boldsymbol{U}}_h^k,$$

where $\mathfrak{R}_{\mathcal{G},T}^k : \boldsymbol{\mathcal{G}}^k(T) \times \boldsymbol{\mathcal{G}}^{\mathrm{c},k}(T) \to \boldsymbol{\mathcal{P}}^k(T;\mathbb{R}^d)$ denotes the recovery operator [17, Eq. (2.17)], which satisfies $\boldsymbol{\pi}_{\mathcal{G},T}^k \mathfrak{R}_{\mathcal{G},T}^k(\boldsymbol{v}_{\mathcal{G},T}, \boldsymbol{v}_{\mathcal{G},T}^{\mathrm{c}}) = \boldsymbol{v}_{\mathcal{G},T}$ and $\boldsymbol{\pi}_{\mathcal{G},T}^{\mathrm{c},k} \mathfrak{R}_{\mathcal{G},T}^k(\boldsymbol{v}_{\mathcal{G},T}, \boldsymbol{v}_{\mathcal{G},T}^{\mathrm{c}}) = \boldsymbol{v}_{\mathcal{G},T}^{\mathrm{c}}$ (where $\boldsymbol{\pi}_{\mathcal{G},T}^{\mathrm{c},k}$ is the L^2-orthogonal projector on $\boldsymbol{\mathcal{G}}^{\mathrm{c},k}(T)$. It can be checked that the discrete divergence (18) and the Darcy potential (19) only depend on the polynomial components shared by $\underline{\boldsymbol{U}}_T^k$ and $\underline{\boldsymbol{X}}_{\mathrm{div},T}^k$, and that they coincide with the corresponding DDR operators respectively defined by [17, Eqs. (3.32) and (4.9)–(4.10)].

Accounting for the previous remark and recalling [17, Eq. (4.12) and (4.13)], it holds

$$\boldsymbol{\pi}_{\mathcal{P},T}^{k-1} \boldsymbol{P}_{\mathrm{D},T}^k \underline{\boldsymbol{v}}_T = \boldsymbol{\pi}_{\mathcal{P},T}^{k-1} \boldsymbol{v}_T \qquad \forall \underline{\boldsymbol{v}}_T \in \underline{\boldsymbol{U}}_T^k, \tag{20}$$

$$\boldsymbol{P}_{\mathrm{D},T}^k \underline{\boldsymbol{I}}_T^k \boldsymbol{v} = \boldsymbol{v} \qquad \forall \boldsymbol{v} \in \boldsymbol{\mathcal{P}}^k(T;\mathbb{R}^d). \tag{21}$$

The approximation properties of $\boldsymbol{P}_{\mathrm{D},T}^k$ in the L^2-norm have been studied in [17, Theorem 6]. The following proposition extends the above results to general Hilbert seminorms.

Proposition 5 (Approximation properties of the Darcy potential)**.** *Let an integer $r \in \{0,\dots,k\}$ be given. Then, for all $T \in \mathcal{T}_h$, all $\boldsymbol{v} \in \boldsymbol{H}^{r+1}(T;\mathbb{R}^d)$, and all $m \in \{0,\dots,r+1\}$,*

$$|\boldsymbol{v} - \boldsymbol{P}_{\mathrm{D},T}^k \underline{\boldsymbol{I}}_T^k \boldsymbol{v}|_{\boldsymbol{H}^m(T;\mathbb{R}^d)} \lesssim h_T^{r+1-m} |\boldsymbol{v}|_{\boldsymbol{H}^{r+1}(T;\mathbb{R}^d)}. \tag{22}$$

Proof. By [19, Proposition 1.35], $\boldsymbol{P}^k_{\mathrm{D},T} \circ \underline{\boldsymbol{I}}^k_T : \boldsymbol{H}^1(T;\mathbb{R}^d) \to \boldsymbol{\mathcal{P}}^k(T;\mathbb{R}^d)$ is a projector owing to (21). By [19, Lemma 1.43], it then suffices to prove that, for all $\boldsymbol{v} \in \boldsymbol{H}^1(T;\mathbb{R}^d)$,

$$\|\boldsymbol{P}^k_{\mathrm{D},T}\underline{\boldsymbol{I}}^k_T\boldsymbol{v}\|_{\boldsymbol{L}^2(T;\mathbb{R}^d)} \lesssim \|\boldsymbol{v}\|_{\boldsymbol{L}^2(T;\mathbb{R}^d)} + h_T|\boldsymbol{v}|_{\boldsymbol{H}^1(T;\mathbb{R}^d)} \qquad \text{if } m = 0, \tag{23}$$

$$|\boldsymbol{P}^k_{\mathrm{D},T}\underline{\boldsymbol{I}}^k_T\boldsymbol{v}|_{\boldsymbol{H}^1(T;\mathbb{R}^d)} \lesssim |\boldsymbol{v}|_{\boldsymbol{H}^1(T;\mathbb{R}^d)} \qquad \text{if } m \geq 1. \tag{24}$$

To prove (23), it suffices to recall Remark 4 and use [18, Eqs. (4.24) and (4.28)]. To prove (24), we write

$$\begin{aligned}
|\boldsymbol{P}^k_{\mathrm{D},T}\underline{\boldsymbol{I}}^k_T\boldsymbol{v}|_{\boldsymbol{H}^1(T;\mathbb{R}^d)} &= |\boldsymbol{P}^k_{\mathrm{D},T}\underline{\boldsymbol{I}}^k_T(\boldsymbol{v} - \boldsymbol{\pi}^0_{\boldsymbol{\mathcal{P}},T}\boldsymbol{v})|_{\boldsymbol{H}^1(T;\mathbb{R}^d)} \\
&\lesssim h_T^{-1}\|\boldsymbol{P}^k_{\mathrm{D},T}\underline{\boldsymbol{I}}^k_T(\boldsymbol{v} - \boldsymbol{\pi}^0_{\boldsymbol{\mathcal{P}},T}\boldsymbol{v})\|_{\boldsymbol{L}^2(T;\mathbb{R}^d)} && \text{[19, Eq. (1.46)]} \\
&\lesssim h_T^{-1}\|\boldsymbol{v} - \boldsymbol{\pi}^0_{\boldsymbol{\mathcal{P}},T}\boldsymbol{v}\|_{\boldsymbol{L}^2(T;\mathbb{R}^d)} + |\boldsymbol{v} - \boldsymbol{\pi}^0_{\boldsymbol{\mathcal{P}},T}\boldsymbol{v}|_{\boldsymbol{H}^1(T;\mathbb{R}^d)} && \text{Eq. (23)} \\
&\lesssim |\boldsymbol{v}|_{\boldsymbol{H}^1(T;\mathbb{R}^d)},
\end{aligned}$$

where the first line follows using the polynomial consistency (21) of $\boldsymbol{P}^k_{\mathrm{D},T}$ to write $0 = |\boldsymbol{\pi}^0_{\boldsymbol{\mathcal{P}},T}\boldsymbol{v}|_{\boldsymbol{H}^1(T;\mathbb{R}^d)} = |\boldsymbol{P}^k_{\mathrm{D},T}\underline{\boldsymbol{I}}^k_T\boldsymbol{\pi}^0_{\boldsymbol{\mathcal{P}},T}\boldsymbol{v}|_{\boldsymbol{H}^1(T;\mathbb{R}^d)}$, while the conclusion follows from a Poincaré–Wirtinger inequality on the zero-average function $\boldsymbol{v} - \boldsymbol{\pi}^0_{\boldsymbol{\mathcal{P}},T}\boldsymbol{v}$. □

Let $\widetilde{\boldsymbol{P}}^k_{\mathrm{D},T} : \underline{\boldsymbol{U}}^k_T \to \boldsymbol{\mathcal{P}}^k(T;\mathbb{R}^d)$ be such that

$$\widetilde{\boldsymbol{P}}^k_{\mathrm{D},T}\underline{\boldsymbol{v}}_T \coloneqq \langle C_{\mathrm{f},T} < 1\rangle \boldsymbol{v}_T + \langle C_{\mathrm{f},T} \geq 1\rangle \boldsymbol{P}^k_{\mathrm{D},T}\underline{\boldsymbol{v}}_T \qquad \forall \underline{\boldsymbol{v}}_T \in \underline{\boldsymbol{U}}^k_T. \tag{25}$$

The Darcy term in (2a) is discretised by means of the bilinear form $a_{\nu,h} : \underline{\boldsymbol{U}}^k_h \times \underline{\boldsymbol{U}}^k_h \to \mathbb{R}$ such that, for all $(\underline{\boldsymbol{w}}_h, \underline{\boldsymbol{v}}_h) \in \underline{\boldsymbol{U}}^k_h \times \underline{\boldsymbol{U}}^k_h$,

$$a_{\nu,h}(\underline{\boldsymbol{w}}_h, \underline{\boldsymbol{v}}_h) \coloneqq \sum_{T\in\mathcal{T}_h} \nu_T a_{\mathrm{D},T}(\underline{\boldsymbol{w}}_T, \underline{\boldsymbol{v}}_T) \tag{26}$$

with, for all $T \in \mathcal{T}_h$,

$$a_{\mathrm{D},T}(\underline{\boldsymbol{w}}_T, \underline{\boldsymbol{v}}_T) \coloneqq \int_T \widetilde{\boldsymbol{P}}^k_{\mathrm{D},T}\underline{\boldsymbol{w}}_T \cdot \widetilde{\boldsymbol{P}}^k_{\mathrm{D},T}\underline{\boldsymbol{v}}_T + \min(1, C_{\mathrm{f},T})(\underline{\boldsymbol{w}}_T - \underline{\boldsymbol{I}}^k_T\boldsymbol{P}^k_{\mathrm{D},T}\underline{\boldsymbol{w}}_T, \underline{\boldsymbol{v}}_T - \underline{\boldsymbol{I}}^k_T\boldsymbol{P}^k_{\mathrm{D},T}\underline{\boldsymbol{v}}_T,)_{\boldsymbol{U},T}. \tag{27}$$

We define the following induced norms: For all $\underline{\boldsymbol{v}}_h \in \underline{\boldsymbol{U}}^k_h$,

$$\|\underline{\boldsymbol{v}}_h\|_{\nu,h} \coloneqq a_{\nu,h}(\underline{\boldsymbol{v}}_h, \underline{\boldsymbol{v}}_h)^{1/2} \quad \text{and} \quad \|\underline{\boldsymbol{v}}_T\|_{\mathrm{D},T} \coloneqq a_{\mathrm{D},T}(\underline{\boldsymbol{v}}_T, \underline{\boldsymbol{v}}_T)^{1/2} \text{ for all } T \in \mathcal{T}_h. \tag{28}$$

3.4 Coupling

The coupling terms in (2a) and (2b) are discretised by the bilinear form $b_h : \underline{\boldsymbol{U}}^k_h \times \boldsymbol{\mathcal{P}}^k(\mathcal{T}_h) \to \mathbb{R}$ such that, for all $(\underline{\boldsymbol{v}}_h, q_h) \in \underline{\boldsymbol{U}}^k_h \times \boldsymbol{\mathcal{P}}^k(\mathcal{T}_h)$,

$$b_h(\underline{\boldsymbol{v}}_h, q_h) \coloneqq -\sum_{T\in\mathcal{T}_h} \int_T D^k_T\underline{\boldsymbol{v}}_T \, q_T, \tag{29}$$

where q_T denotes the restriction of q_h to T. Recalling [19, Eq. (8.36)], it holds: For all $\boldsymbol{v} \in \boldsymbol{H}^1(\Omega;\mathbb{R}^d)$,

$$b_h(\underline{\boldsymbol{I}}^k_h\boldsymbol{v}, q_h) = -\int_\Omega \boldsymbol{\nabla}\cdot\boldsymbol{v} \, q_h \qquad \forall q_h \in \boldsymbol{\mathcal{P}}^k(\mathcal{T}_h). \tag{30}$$

3.5 Discrete problem and main results

The discrete problem reads: Find $(\underline{\boldsymbol{u}}_h, p_h) \in \underline{\boldsymbol{U}}_{h,0}^k \times P_h^k$ such that

$$\begin{aligned} a_{\mu,h}(\underline{\boldsymbol{u}}_h, \underline{\boldsymbol{v}}_h) + a_{\nu,h}(\underline{\boldsymbol{u}}_h, \underline{\boldsymbol{v}}_h) + b_h(\underline{\boldsymbol{v}}_h, p_h) &= \sum_{T\in\mathcal{T}_h} \int_T \boldsymbol{f}\cdot \widetilde{\boldsymbol{P}}_{\mathrm{D},T}^k \underline{\boldsymbol{v}}_T \qquad && \forall \underline{\boldsymbol{v}}_h \in \underline{\boldsymbol{U}}_{h,0}^k, \\ -b_h(\underline{\boldsymbol{u}}_h, q_h) &= \int_\Omega g q_h && \forall q_h \in P_h^k. \end{aligned} \tag{31}$$

The equivalent variational formulation is: Find $(\underline{\boldsymbol{u}}_h, p_h) \in \underline{\boldsymbol{U}}_{h,0}^k \times P_h^k$ such that

$$\mathcal{A}_h((\underline{\boldsymbol{u}}_h, p_h), (\underline{\boldsymbol{v}}_h, q_h)) = \sum_{T\in\mathcal{T}_h} \int_T \boldsymbol{f}\cdot \widetilde{\boldsymbol{P}}_{\mathrm{D},T}^k \underline{\boldsymbol{v}}_T + \int_\Omega g q_h, \tag{32}$$

with $\mathcal{A}_h : \left(\underline{\boldsymbol{U}}_h^k \times P_h^k\right)^2 \to \mathbb{R}$ such that, for all $(\underline{\boldsymbol{w}}_h, r_h)$ and all $(\underline{\boldsymbol{v}}_h, q_h)$ in $\underline{\boldsymbol{U}}_h^k \times P_h^k$,

$$\mathcal{A}_h((\underline{\boldsymbol{w}}_h, r_h), (\underline{\boldsymbol{v}}_h, q_h)) \coloneqq a_{\mu,h}(\underline{\boldsymbol{w}}_h, \underline{\boldsymbol{v}}_h) + a_{\nu,h}(\underline{\boldsymbol{w}}_h, \underline{\boldsymbol{v}}_h) + b_h(\underline{\boldsymbol{v}}_h, r_h) - b_h(\underline{\boldsymbol{w}}_h, q_h). \tag{33}$$

Recalling (13) and (28), we equip the space $\underline{\boldsymbol{U}}_{h,0}^k$ with the following natural energy norm: For all $\underline{\boldsymbol{v}}_h \in \underline{\boldsymbol{U}}_{h,0}^k$,

$$\|\underline{\boldsymbol{v}}_h\|_{\mu,\nu,h} \coloneqq \left(\|\underline{\boldsymbol{v}}_h\|_{\mu,h}^2 + \|\underline{\boldsymbol{v}}_h\|_{\nu,h}^2\right)^{1/2} \tag{34}$$

and, given a linear form $\ell_h : \underline{\boldsymbol{U}}_{h,0}^k \to \mathbb{R}$, we denote its dual norm by

$$\|\ell_h\|_{\mu,\nu,h,*} \coloneqq \sup_{\underline{\boldsymbol{v}}_h \in \underline{\boldsymbol{U}}_{h,0}^k \setminus \{\underline{\boldsymbol{0}}\}} \frac{\ell_h(\underline{\boldsymbol{v}}_h)}{\|\underline{\boldsymbol{v}}_h\|_{\mu,\nu,h}}.$$

The bilinear form $a_{\mu,h} + a_{\nu,h}$ is $\|\cdot\|_{\mu,\nu,h}$-coercive with unit coercivity constant. The well-posedness of (31) then classically follows from the theory of mixed methods (see, e.g., [19, Lemma A.11]) thanks to the inf-sup condition on b_h stated in the following lemma.

Lemma 6 (Inf-sup condition on b_h)**.** *Letting $\beta \coloneqq (\overline{\mu} + \overline{\nu})^{-1/2}$, it holds, for all $q_h \in P_h^k$,*

$$\beta \|q_h\|_{L^2(\Omega)} \lesssim \sup_{\underline{\boldsymbol{v}}_h \in \underline{\boldsymbol{U}}_{h,0}^k \setminus \{\underline{\boldsymbol{0}}\}} \frac{b_h(\underline{\boldsymbol{v}}_h, q_h)}{\|\underline{\boldsymbol{v}}_h\|_{\mu,\nu,h}}.$$

Proof. See Section 5.1. □

Thanks to the presence of cut-off factors, the following error estimate is robust across the entire range of (local) regimes.

Theorem 7 (Error estimate)**.** *Denote by $(\boldsymbol{u}, p) \in \boldsymbol{H}_0^1(\Omega;\mathbb{R}^d) \times L_0^2(\Omega)$ the unique solution to the standard weak formulation of (2) and by $(\underline{\boldsymbol{u}}_h, p_h) \in \underline{\boldsymbol{U}}_{h,0}^k \times P_h^k$ the unique solution of the numerical scheme (31) (or, equivalently, (32)). Then, recalling the notation (5) for the truth value*

of a logical proposition and assuming, for some $r \in \{0, \ldots, k\}$, $\boldsymbol{u} \in \boldsymbol{H}^{r+2}(\mathcal{T}_h; \mathbb{R}^d)$, $p \in H^1(\Omega)$, *and, for all* $T \in \mathcal{T}_h$, $p \in H^{r+1+\langle C_{\mathrm{f},T} \geq 1\rangle}(T)$, *it holds,*

$$\begin{aligned}
&\|\underline{\boldsymbol{u}}_h - \underline{\boldsymbol{I}}_h^k \boldsymbol{u}\|_{\mu,\nu,h}^2 + \|p_h - \pi_{\mathcal{P},h}^k p\|_{L^2(\Omega)}^2 \\
&\quad \lesssim \frac{1}{\gamma^2}\Bigg[\sum_{T\in\mathcal{T}_h} \mu_T \min(1, C_{\mathrm{f},T}^{-1}) h_T^{2(r+1)} |\boldsymbol{u}|_{\boldsymbol{H}^{r+2}(T;\mathbb{R}^d)}^2 + \sum_{T\in\mathcal{T}_h} \nu_T \min(1, C_{\mathrm{f},T}) h_T^{2(r+1)} |\boldsymbol{u}|_{\boldsymbol{H}^{r+1}(T;\mathbb{R}^d)}^2 \\
&\qquad + \sum_{T\in\mathcal{T}_h} \left(\mu_T^{-1} \langle C_{\mathrm{f},T} < 1\rangle h_T^{2(r+1)} |p|_{H^{r+1}(T)}^2 + \nu_T^{-1} \langle C_{\mathrm{f},T} \geq 1\rangle h_T^{2(r+1)} |p|_{H^{r+2}(T)}^2 \right) \Bigg],
\end{aligned} \tag{35}$$

where $\gamma^{-2} \coloneqq 4\beta^{-4} + 8\beta^{-2} + 1$ *with* β *as in Lemma 6, while, for all* $T \in \mathcal{T}_h$, $\nu_T^{-1}\langle C_{\mathrm{f},T} \geq 1\rangle \coloneqq 0$ *if* $\nu_T = 0$.

Proof. See Section 5.2. □

Remark 8 (Robustness of the error estimate and application to the Darcy problem). In the spirit of [10, Remark 13], the presence of the cutoff factors $\min(1, C_{\mathrm{f},T}^{-1})$, $\min(1, C_{\mathrm{f},T})$, $\mu_T^{-1}\langle C_{\mathrm{f},T} < 1\rangle$, and $\nu_T^{-1}\langle C_{\mathrm{f},T} \geq 1\rangle$ makes the above estimate robust across the entire range $C_{\mathrm{f},T} \in [0, +\infty)$.

The case $C_{\mathrm{f},T} = +\infty$ corresponds to the pure Darcy problem, which is the singular limit obtained assuming $\min_\Omega \nu > 0$ and $C_{\mathrm{f},T} = +\infty$ for all $T \in \mathcal{T}_h$. In this case, a more in-depth discussion is in order. Denoting by $\gamma_{\boldsymbol{n}}$ the normal trace operator on $\partial\Omega$, the space for the velocity becomes $\boldsymbol{H}_0(\mathrm{div};\Omega) \coloneqq \{\boldsymbol{v} \in \boldsymbol{H}(\mathrm{div};\Omega) \,:\, \gamma_{\boldsymbol{n}}(\boldsymbol{v}) = 0 \text{ on } \partial\Omega\}$, and the weak formulation of (2) yields the Darcy problem in mixed form. The error estimate (35) remains valid under the regularity assumption $\boldsymbol{u} \in \boldsymbol{H}^{r+1}(\mathcal{T}_h; \mathbb{R}^d)$, and provided the following conventions are adopted: $\mu_T^{-1}\langle C_{\mathrm{f},T} < 1\rangle \coloneqq 0$ and, for any $\boldsymbol{v} \in \boldsymbol{H}_0(\mathrm{div};\Omega) \cap \boldsymbol{H}^1(\mathcal{T}_h;\mathbb{R}^d)$, all the components of the boundary values of $\underline{\boldsymbol{I}}_h^k \boldsymbol{v}$ are forced to zero, i.e., $(\underline{\boldsymbol{I}}_h^k \boldsymbol{v})_F \coloneqq \boldsymbol{0}$ for all $F \in \mathcal{F}_h^{\mathrm{b}}$. Notice that the tangential components of the velocity on boundary faces do not appear in the formulation of the method when $\mu = 0$. To check this fact:

- Concerning the Darcy contribution $a_{\mathrm{D},T}$ (cf. (27)), recall Remark 4 for the consistent term while, for the stabilisation term, notice that, by (6), boundary faces are not present in $(\cdot,\cdot)_{\boldsymbol{U},T}$ since $C_{\mathrm{f},T} \geq 1$ for all $T \in \mathcal{T}_h$;
- Concerning the coupling term b_h (cf. (29)), notice that the following equivalent formulation results applying the definition (9) of $\boldsymbol{G}_T^k$ with $\boldsymbol{\tau} = q_T \boldsymbol{I}_d \coloneqq (q_h)_{|T} \boldsymbol{I}_d$ for all $T \in \mathcal{T}_h$:

$$b_h(\underline{\boldsymbol{v}}_h, q_h) = \sum_{T\in\mathcal{T}_h} \left(\int_T \boldsymbol{v}_T \cdot \boldsymbol{\nabla} q_T - \sum_{F\in\mathcal{F}_T} \omega_{TF} \int_F (\boldsymbol{v}_F \cdot \boldsymbol{n}_F)\, q_T \right),$$

  clearly showing that b_h is independent of the tangential component of $\boldsymbol{v}_F$ for all $F \in \mathcal{F}_h$.

The method obtained for the pure Darcy problem has more unknowns than, say, the mixed method of [22] or a similar one that could be obtained starting from the space $\underline{\boldsymbol{X}}_{\mathrm{div},h}^k$ of [17]. In particular, the tangential components of interface unknowns are not present in the consistency term of $a_{\mathrm{D},T}$ (see again Remark 4), but are controlled by the stabilisation term. Despite this difference in the discrete space for the flux, the estimate for the error on $\boldsymbol{u}$ resulting from (35) in the pure Darcy case is analogous to the one given in [22, Theorem 6] (where the highest regularity case corresponding to $r = k$ is considered).

4 Numerical tests

In this section we numerically assess the convergence properties of the scheme (31) for different values of the friction coefficient (including the limit cases) and on both standard and genuinely polyhedral meshes.

The code used for the numerical tests is part of the open source C++ `HArDCore3D` library; see https://github.com/jdroniou/HArDCore. In order to reduce the size of the global linear systems, static condensation was applied the scheme (31) in accordance with the principles outlined in [19, Appendix B]; see [24, Section 6] for a discussion specific to the Stokes equations and [9] for a study of the effect of static condensation on p-multilevel preconditioners for the Stokes problem. We have chosen to locally eliminate all element degrees of freedom except for the average value of the pressure inside each element. The linear systems were solved using the `Intel MKL PARDISO` library (see https://software.intel.com/en-us/mkl).

The parameter λ_T in (6) was chosen as $\frac{h_T^3}{|T|}\operatorname{card}(\mathcal{F}_T)$, to give a larger weight to the element contribution in (7) when T is elongated or has many faces: this compensates the relatively larger contribution, in these circumstances, of the boundary terms in this local norm. We have also applied scalings to the stabilisation terms in (12) and (27): 3 for the Stokes stabilisation, 0.3 for the Darcy stabilisation. Introducing scalings in the stabilisation terms is not strictly necessary to observe the convergence of the scheme at the expected rates, but we noticed that they improve the magnitudes of the relative errors. Understanding the optimal scaling of stabilisations involved in polytopal methods is an ongoing subject of investigation; here, these numbers were found by quick trial and error on unexpensive tests (low degree k, coarse meshes), before being used in all the tests below.

4.1 Convergence in various regimes

Following [10], we consider a constant viscosity μ and inverse permeability ν, and we evaluate the relative velocity–pressure error

$$E_{\boldsymbol{u},p} = \frac{\left(\|\underline{\boldsymbol{u}}_h - \underline{\boldsymbol{I}}_h^k \boldsymbol{u}\|_{\mu,\nu,h}^2 + \|p_h - \pi_{\mathcal{P},h}^k p\|_{L^2(\Omega)}^2\right)^{1/2}}{\left(\|\underline{\boldsymbol{I}}_h^k \boldsymbol{u}\|_{\mu,\nu,h}^2 + \|\pi_{\mathcal{P},h}^k p\|_{L^2(\Omega)}^2\right)^{1/2}},$$

when the nature of the exact solution $(\boldsymbol{u}, p)$ is determined by the global friction coefficient $C_{\mathrm{f},\Omega} = \nu/\mu$, with the convention $C_{\mathrm{f},\Omega} = +\infty$ if $\mu = 0$. Specifically, we consider the domain $\Omega = (0,1)^3$ and, setting $\chi_{\mathrm{S}}(C_{\mathrm{f},\Omega}) \coloneqq \exp(-C_{\mathrm{f},\Omega})$, the pressure and velocity are chosen as

$$\begin{aligned} p(x,y,z) &= \sin(2\pi x)\sin(2\pi y)\sin(2\pi z) \quad \forall (x,y,z) \in \Omega, \\ \boldsymbol{u} &= \chi_{\mathrm{S}}(C_{\mathrm{f},\Omega})\boldsymbol{u}_{\mathrm{S}} + (1 - \chi_{\mathrm{S}}(C_{\mathrm{f},\Omega}))\boldsymbol{u}_{\mathrm{D}}, \end{aligned}$$

where $\boldsymbol{u}_{\mathrm{S}}$ and $\boldsymbol{u}_{\mathrm{D}}$ are the velocity obtained in the Stokes ($C_{\mathrm{f},\Omega} = 0$) and Darcy ($C_{\mathrm{f},\Omega} = +\infty$) limits, and are given by

$$\boldsymbol{u}_{\mathrm{S}}(x,y,z) = \frac{1}{2}\begin{bmatrix} \sin(2\pi x)\cos(2\pi y)\cos(2\pi z) \\ \cos(2\pi x)\sin(2\pi y)\cos(2\pi z) \\ -2\cos(2\pi x)\cos(2\pi y)\sin(2\pi z) \end{bmatrix} \quad \forall (x,y,z) \in \Omega,$$

$$\boldsymbol{u}_{\mathrm{D}} = \begin{cases} -\nu^{-1}\boldsymbol{\nabla} p & \text{if } \nu > 0, \\ \boldsymbol{0} & \text{otherwise.} \end{cases}$$

We notice that $\nabla \cdot \boldsymbol{u}_S = 0$ and that $\nu \boldsymbol{u}_D + \nabla p = 0$; these are expected relations, respectively, for a solution of an incompressible Stokes equation, and for a solution of a Darcy equation in mixed form (when gravity is neglected). The meshes used for the test correspond to the families of Voronoi meshes "Voro-small-0", of tetrahedral meshes "Tetgen-Cube-0" and of random hexahedral meshes "Random-Hexahedra" available on the `HArDCore3D` repository. The errors as a function of h are presented in Figures 1, 2 and 3, showing that the predicted convergence is observed in practice for all the considered mesh families and polynomial degrees, and that both orders of convergence and magnitudes of errors are robust in all regimes.

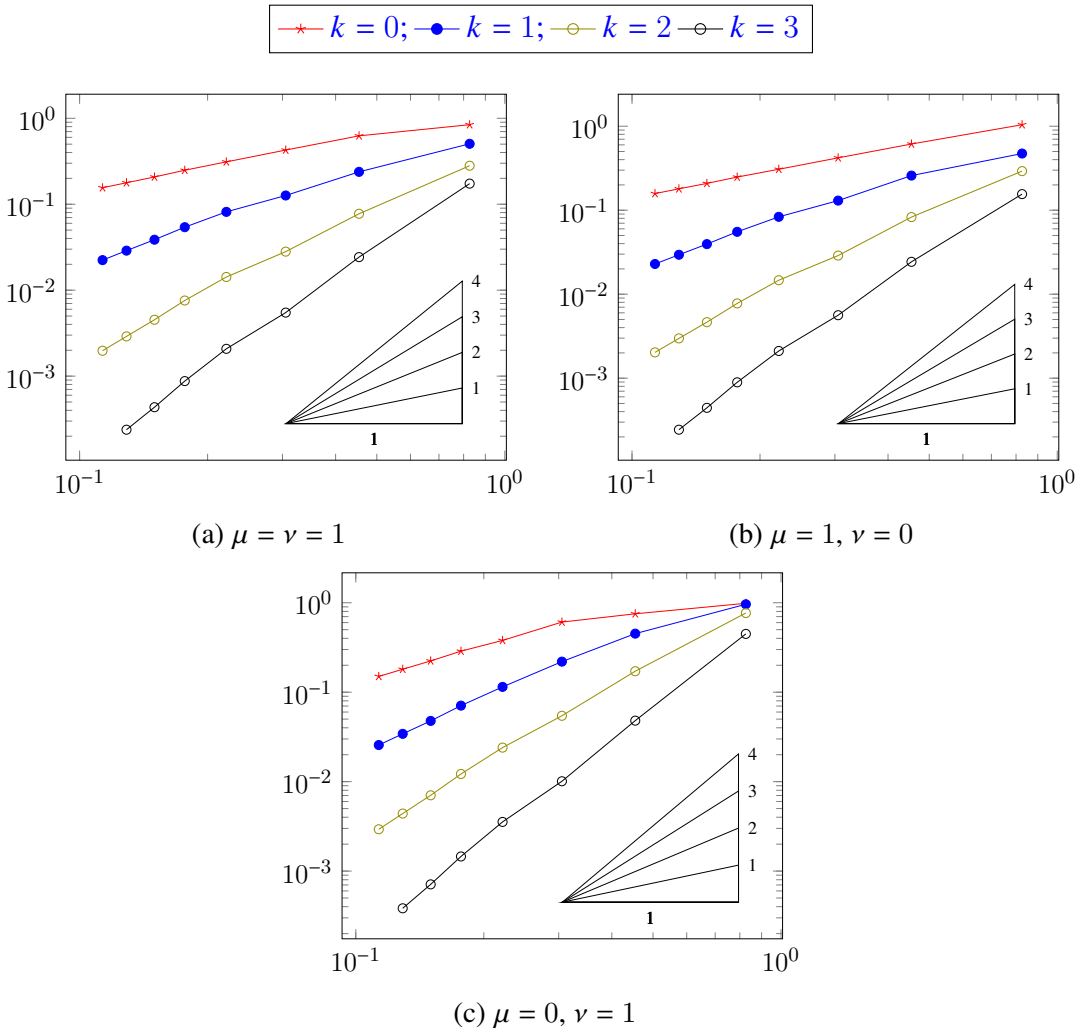

(a) $\mu = \nu = 1$

(b) $\mu = 1, \nu = 0$

(c) $\mu = 0, \nu = 1$

Figure 1: Voronoi meshes: errors $E_{u,p}$ with respect to h

4.2 Lid-driven cavity in porous medium

The tests in this section are inspired by situations described in [1, 6]. In these references, a V-crack is realised at the top of a homogeneous porous medium, and plays the role of a lid-driven cavity (with a Stokes-dominated model in this cavity, while the rest of the medium is modelled using pure Darcy flow), and low-order mixed finite elements on triangles/tetrahedra are used to simulate the flow.

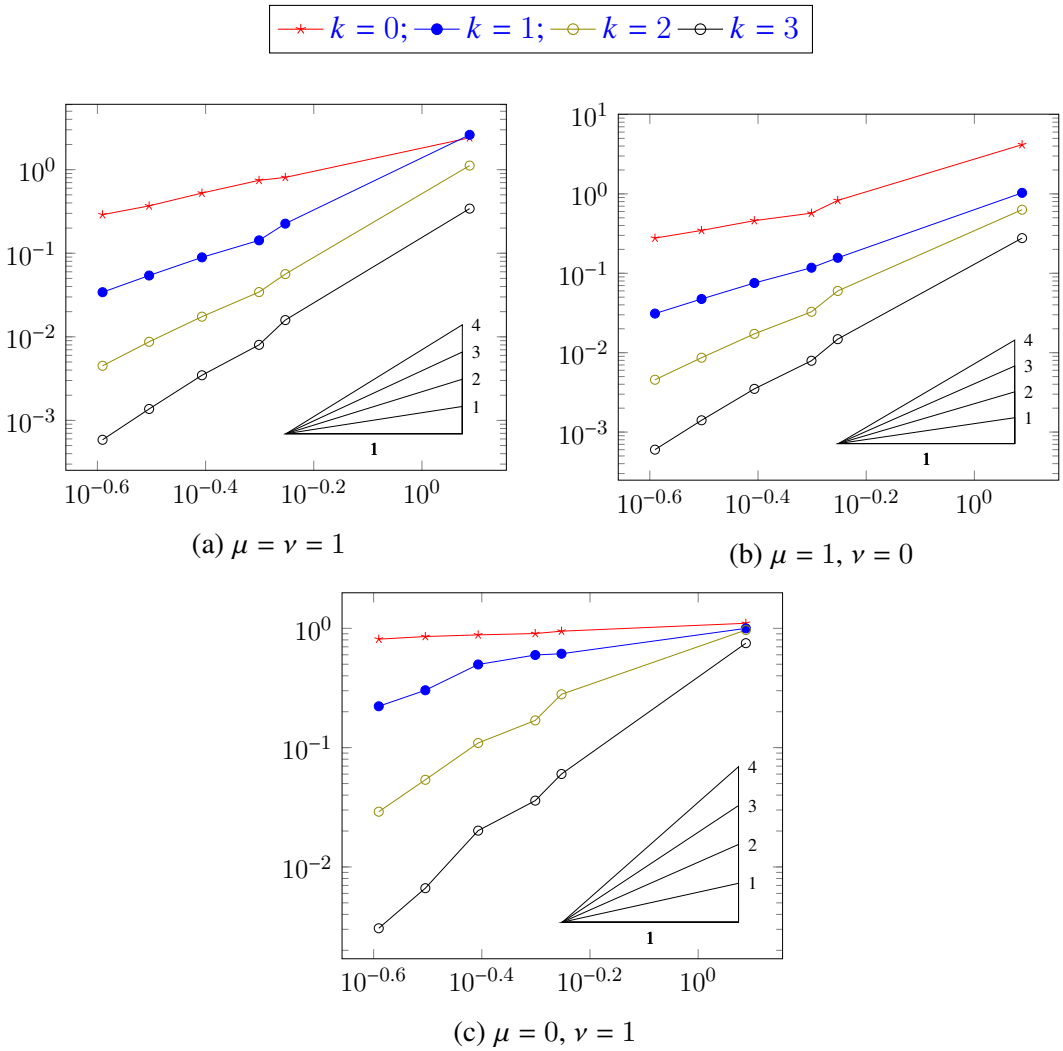

(a) $\mu = \nu = 1$

(b) $\mu = 1$, $\nu = 0$

(c) $\mu = 0$, $\nu = 1$

Figure 2: Tetrahedral meshes: errors $E_{u,p}$ with respect to h

We consider here a cavity, where a pure Stokes flow occurs, sitting in a porous medium, with pure Darcy flow; the porous medium is heterogeneous, with permeability equal to 10^{-7} in the surrounding "box" and 10^{-2} in a "wedge" at the outset of the cavity; see Figure 4, left. The domain is $\Omega = (-1, 2) \times (-1, 2) \times (-2, 0)$, with the cavity being $(0, 1)^3$ and the wedge $\{(x, y, z) \in \mathbb{R}^3 \,:\, 1 < x < 2\,,\ 0 < y < 1\,,\ -0.75(x-1) + 0.25 < z < 0\}$. The domain has been meshed using `gmsh` (https://gmsh.info/), with cubic elements in the cavity, and mostly tetrahedral elements in the porous medium (together with a few pyramidal elements at the junctions cavity–porous medium); see Figure 4, right, for an example of mesh, and Table 1 for the characteristic of all meshes. The files describing the geometry are available in the `HArDCore` repository.

The forcing term $\boldsymbol{f} = (0, 0, -0.98)$ represents the gravity, while we fix $g = 0$. The boundary conditions on the velocity are $\boldsymbol{u}(x, y, z) = (x(1-x), 0, 0)$ on top of the cavity, and $\boldsymbol{u} = \boldsymbol{0}$ elsewhere. Figure 5 presents the streamlines obtained on the third mesh in the family with $k = 2$. These streamlines show the usual form of circulation inside the cavity for a pure Stokes lid-driven cavity, which drives some (slower) motion inside the wedge section of the porous medium; given the very low permeability of the rest of the medium, little material is transferred

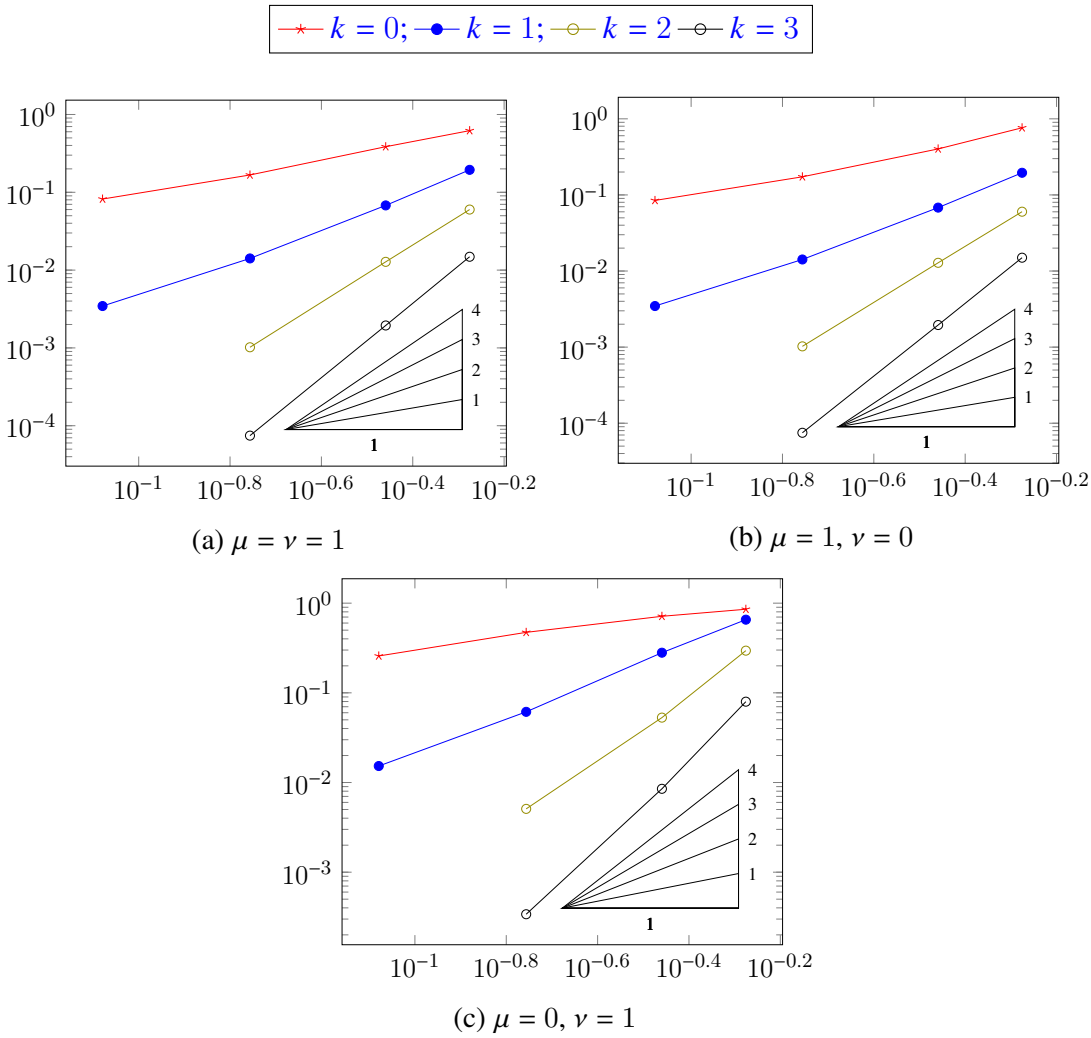

(a) $\mu = \nu = 1$

(b) $\mu = 1, \nu = 0$

(c) $\mu = 0, \nu = 1$

Figure 3: Random hexahedral meshes: errors $E_{u,p}$ with respect to h

into this medium, in which the velocity remains almost zero; in the region $z < -1$ below the cavity, for example, the maximum of the vertex values (obtained by averaging the potential reconstructions in each element surrounding the vertices) of the velocity is below 6×10^{-5}.

To qualitatively assess the impact of increasing the degree of approximation k of the method, we evaluate for various meshes and degrees the flux across the interface $\Gamma = \{0\} \times (0,1) \times (-0.75, 1)$ between the cavity and the wedge. All the meshes $\mathcal{M}_h$ we consider are compatible with this interface, that is, setting $\Gamma_h = \{F \in \mathcal{F}_h : F \subset \Gamma\}$ we have $\Gamma = \cup_{F \in \Gamma_h} F$. We then consider the numerical convergence of the numerical flux defined by

$$\sum_{F \in \Gamma_h} \int_F \boldsymbol{u}_F \cdot \boldsymbol{n}_\Gamma,$$

where $\boldsymbol{n}_\Gamma = (1,0,0)$ is the unit normal to Γ pointing inside the wedge. The values of this flux for different degrees of approximations k are provided in Figure 6 (left: w.r.t. the mesh size; right: w.r.t. the total wall time, including assembly and solution time – notice that the `HArDCore` library uses multi-threading processes). These results show that the lowest order of

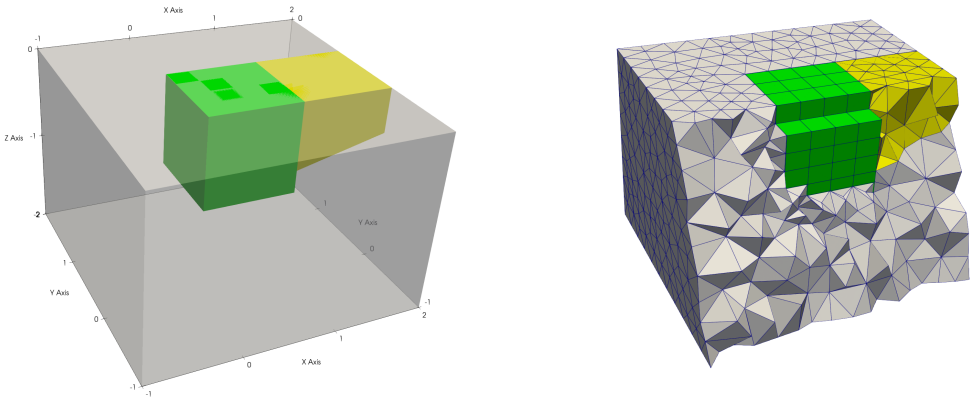

Figure 4: Left: geometry of the cavity (green) inside the porous medium, comprising a wedge (green) and the surrounding box (shadow). Right: example of mesh used in the simulations.

Mesh index	1	2	3	4	5
Mesh size	0.95	0.61	0.54	0.22	0.17
Num. of elements	1,326	5,935	7,963	99,748	201,653

Table 1: Characteristics of the mesh family for the tests in Section 4.2.

approximation struggles to provide what seems to be a correct value of the flux, and that the mesh must be extremely fine to get close to this value; on the contrary, for $k \geq 1$, all results, even on coarse meshes and with a low computational cost, seem to be very close to a given value, indicating that convergence has already occurred in these cases. These results corroborate a conclusion already highlighted in [3]: even on a problem where the solution is not expected to be very regular, slightly increasing the order of approximation of the scheme (here, going from $k = 0$ to $k = 1$) can lead to a vastly improved accuracy of the numerical outputs at a very low computational cost.

5 Analysis

5.1 Stability

Proposition 9 ($\|\cdot\|_{\mu,\nu,h}$-boundedness of the interpolator)**.** *With β as in Lemma 6, it holds, for all $\boldsymbol{v} \in \boldsymbol{H}^1(\Omega;\mathbb{R}^d)$,*

$$\beta\|\underline{\boldsymbol{I}}_h^k \boldsymbol{v}\|_{\mu,\nu,h} \lesssim \|\boldsymbol{v}\|_{\boldsymbol{H}^1(\Omega;\mathbb{R}^d)}. \tag{36}$$

Proof. It holds, by definition, $\|\underline{\boldsymbol{I}}_h^k \boldsymbol{v}\|_{\mu,\nu,h}^2 = \sum_{T\in\mathcal{T}_h} [\mu_T \mathfrak{T}_1(T) + \nu_T \mathfrak{T}_2(T) + \nu_T \mathfrak{T}_3(T)]$ with

$$\mathfrak{T}_1(T) \coloneqq \|\boldsymbol{G}_T^k \underline{\boldsymbol{I}}_T^k \boldsymbol{v}\|_{\boldsymbol{L}^2(T;\mathbb{R}^{d\times d})}^2 + \frac{\min(1, C_{\mathrm{f},T}^{-1})}{h_T^2} \|\underline{\boldsymbol{I}}_T^k (\boldsymbol{v} - \boldsymbol{P}_{\mathrm{S},T}^{k+1} \underline{\boldsymbol{I}}_T^k \boldsymbol{v})\|_{\boldsymbol{U},T}^2,$$

$$\mathfrak{T}_2(T) \coloneqq \|\widetilde{\boldsymbol{P}}_{\mathrm{D},T}^k \underline{\boldsymbol{I}}_T^k \boldsymbol{v}\|_{\boldsymbol{L}^2(T;\mathbb{R}^d)}^2, \qquad \mathfrak{T}_3(T) \coloneqq \min(1, C_{\mathrm{f},T}) \|\underline{\boldsymbol{I}}_T^k (\boldsymbol{v} - \boldsymbol{P}_{\mathrm{D},T}^k \underline{\boldsymbol{I}}_T^k \boldsymbol{v})\|_{\boldsymbol{U},T}^2.$$

For the first term, combining (14) and [19, Eqs. (8.25)], we obtain $\mathfrak{T}_1(T) \lesssim |\boldsymbol{v}|_{\boldsymbol{H}^1(T;\mathbb{R}^d)}^2$. For

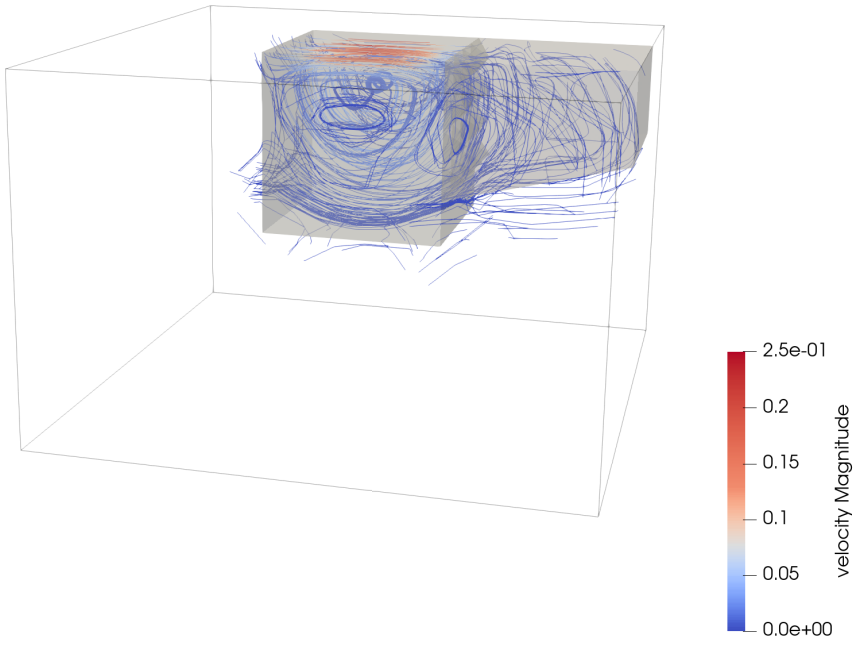

Figure 5: Streamlines for the test case of Section 4.2 (cavity and wedge displayed in shadow).

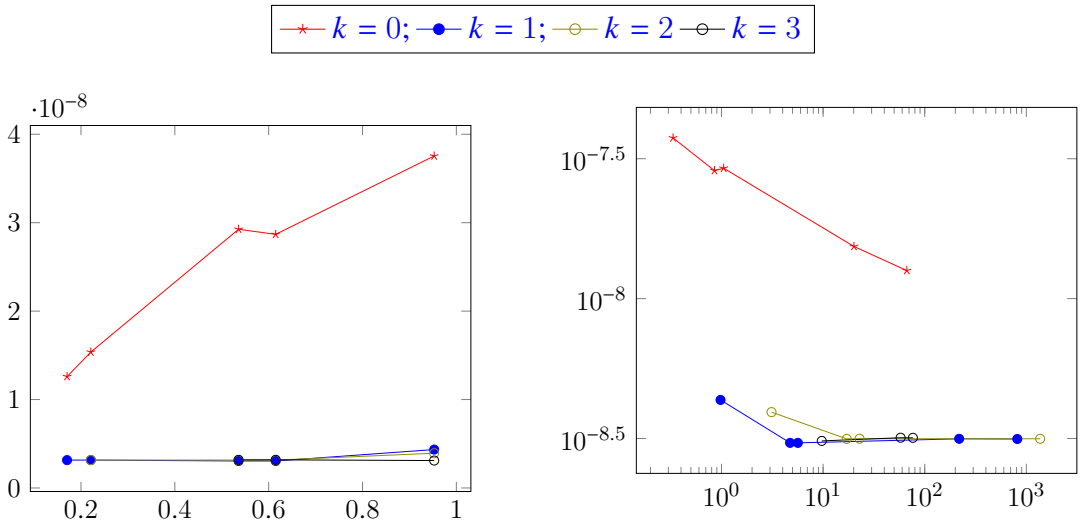

(a) w.r.t. mesh size

(b) w.r.t. wall time (seconds)

Figure 6: Convergence of flux values from the cavity to the wedge.

the second term, if $C_{\mathrm{f},T} < 1$, we can write $\mathfrak{T}_2(T) = \|\boldsymbol{\pi}^k_{\boldsymbol{\mathcal{P}},T}\boldsymbol{v}\|^2_{\boldsymbol{L}^2(T;\mathbb{R}^d)} \le \|\boldsymbol{v}\|^2_{\boldsymbol{L}^2(T;\mathbb{R}^d)}$ using the boundedness of $\boldsymbol{\pi}^k_{\boldsymbol{\mathcal{P}},T}$, while, if $C_{\mathrm{f},T} \ge 1$, (23) gives $\mathfrak{T}_2(T) \lesssim \|\boldsymbol{v}\|^2_{\boldsymbol{L}^2(T;\mathbb{R}^d)} + h_T^2|\boldsymbol{v}|^2_{\boldsymbol{H}^1(T;\mathbb{R}^d)} \le \|\boldsymbol{v}\|^2_{\boldsymbol{H}^1(T;\mathbb{R}^d)}$, where the conclusion follows observing that $h_T \le 1$ since Ω has unit diameter by assumption. Finally, for the third term, the boundedness (8) of the interpolator in the $\|\cdot\|_{U,T}$-norm followed by the approximation properties (22) of $\boldsymbol{P}^k_{\mathrm{D},T} \circ \underline{\boldsymbol{I}}^k_T$ with $(r,m) = (0,0)$ and $(r,m) = (0,1)$ yield

$$\mathfrak{T}_3(T) \lesssim \|\boldsymbol{v} - \boldsymbol{P}^k_{\mathrm{D},T}\underline{\boldsymbol{I}}^k_T\boldsymbol{v}\|^2_{\boldsymbol{L}^2(T;\mathbb{R}^d)} + h_T^2|\boldsymbol{v} - \boldsymbol{P}^k_{\mathrm{D},T}\underline{\boldsymbol{I}}^k_T\boldsymbol{v}|^2_{\boldsymbol{H}^1(T;\mathbb{R}^d)} \lesssim h_T^2|\boldsymbol{v}|^2_{\boldsymbol{H}^1(T;\mathbb{R}^d)}.$$

Gathering the above estimates and recalling the bounds (1) on μ and ν, the result follows. □

Proof of Lemma 6. Classical consequence of the continuous inf-sup condition for the divergence $\boldsymbol{\nabla}\cdot : \boldsymbol{H}^1_0(\Omega;\mathbb{R}^d) \to L^2_0(\Omega)$ (see, e.g., [8, 25, 27, 33]) along with the Fortin properties for the interpolator corresponding to (30) and (36); see, e.g., [7, Section 5.4.3] for further details. □

5.2 Convergence

The purpose of this section is to prove Theorem 7. The proof rests on consistency results for the Stokes, Darcy, and coupling bilinear forms as well as the forcing term linear form which make the object of the following subsections.

5.2.1 Consistency of the Stokes bilinear form

Lemma 10 (Consistency of the Stokes bilinear form)**.** *Given $\boldsymbol{w} \in \boldsymbol{H}^1_0(\Omega;\mathbb{R}^d)$ such that $\boldsymbol{\nabla}\cdot(\mu\boldsymbol{\nabla}\boldsymbol{w}) \in \boldsymbol{L}^2(\Omega;\mathbb{R}^d)$, let the Stokes consistency error linear form $\mathcal{E}^k_{\mathrm{S},h}(\boldsymbol{w};\cdot) : \underline{\boldsymbol{U}}^k_{h,0} \to \mathbb{R}$ be such that, for all $\underline{\boldsymbol{v}}_h \in \underline{\boldsymbol{U}}^k_{h,0}$,*

$$\mathcal{E}^k_{\mathrm{S},h}(\boldsymbol{w};\underline{\boldsymbol{v}}_h) \coloneqq -\sum_{T\in\mathcal{T}_h}\int_T \boldsymbol{\nabla}\cdot(\mu_T\boldsymbol{\nabla}\boldsymbol{w})\cdot\boldsymbol{v}_T - a_{\mu,h}(\underline{\boldsymbol{I}}^k_h\boldsymbol{w},\underline{\boldsymbol{v}}_h). \tag{37}$$

Then, further assuming $\boldsymbol{w} \in \boldsymbol{H}^{r+2}(\mathcal{T}_h;\mathbb{R}^d)$ *for some* $r \in \{0,\dots,k\}$*, it holds*

$$\|\mathcal{E}_{\mathrm{S},h}^k(\boldsymbol{w};\cdot)\|_{\mu,\nu,h,*} \lesssim \left(\sum_{T\in\mathcal{T}_h} \mu_T \min(1, C_{\mathrm{f},T}^{-1}) h_T^{2(r+1)} |\boldsymbol{w}|^2_{\boldsymbol{H}^{r+2}(T;\mathbb{R}^d)}\right)^{1/2}. \tag{38}$$

Proof. Let $\underline{\boldsymbol{v}}_h \in \underline{\boldsymbol{U}}_{h,0}^k \setminus \{\underline{\boldsymbol{0}}\}$. Proceeding as in [19, Point (ii) in Lemma 2.18] using an integration by parts for the first term in the definition of $\mathcal{E}_{\mathrm{S},h}^k$ along with the definitions (11) of $a_{\mu,h}$ and (9) of $\boldsymbol{G}_T^k$ for the second term, we get the following reformulation of the error:

$$\begin{aligned}\mathcal{E}_{\mathrm{S},h}^k(\boldsymbol{w};\underline{\boldsymbol{v}}_h) = \sum_{T\in\mathcal{T}_h}\sum_{F\in\mathcal{F}_T} \omega_{TF} \int_F \mu_T(\boldsymbol{\nabla}\boldsymbol{w} - \boldsymbol{G}_T^k\underline{\boldsymbol{I}}_T^k\boldsymbol{w})\boldsymbol{n}_F\cdot(\boldsymbol{v}_F - \boldsymbol{v}_T)\\ - \sum_{T\in\mathcal{T}_h} \frac{\mu_T\min(1,C_{\mathrm{f},T}^{-1})}{h_T^2}(\underline{\boldsymbol{I}}_T^k(\boldsymbol{w} - \boldsymbol{P}_{\mathrm{S},T}^{k+1}\underline{\boldsymbol{I}}_T^k\boldsymbol{w}), \underline{\boldsymbol{v}}_T - \underline{\boldsymbol{I}}_T^k\boldsymbol{P}_{\mathrm{S},T}^{k+1}\underline{\boldsymbol{v}}_T)_{U,T}.\end{aligned}$$

Using Cauchy–Schwarz and Hölder inequalities along with $\|\boldsymbol{n}_F\|_{\boldsymbol{L}^\infty(F;\mathbb{R}^d)} \le 1$ for all $F\in\mathcal{F}_h$, we can write

$$\mathcal{E}_{\mathrm{S},h}^k(\boldsymbol{w};\underline{\boldsymbol{v}}_h) \lesssim \sum_{T\in\mathcal{T}_h} [\mathfrak{T}_1(T) + \mathfrak{T}_2(T)] \tag{39}$$

with

$$\mathfrak{T}_1(T) \coloneqq \mu_T^{1/2}h_T^{1/2}\|\boldsymbol{\nabla}\boldsymbol{w} - \boldsymbol{G}_T^k\underline{\boldsymbol{I}}_T^k\boldsymbol{w}\|_{\boldsymbol{L}^2(\partial T;\mathbb{R}^{d\times d})}\left(\frac{\mu_T}{h_T}\sum_{F\in\mathcal{F}_T}\|\boldsymbol{v}_F - \boldsymbol{v}_T\|^2_{\boldsymbol{L}^2(F;\mathbb{R}^d)}\right)^{1/2},$$

$$\mathfrak{T}_2(T) \coloneqq \frac{\mu_T\min(1,C_{\mathrm{f},T}^{-1})}{h_T^2}\|\underline{\boldsymbol{I}}_T^k(\boldsymbol{w} - \boldsymbol{P}_{\mathrm{S},T}^{k+1}\underline{\boldsymbol{I}}_T^k\boldsymbol{w})\|_{U,T}\|\underline{\boldsymbol{v}}_T - \underline{\boldsymbol{I}}_T^k\boldsymbol{P}_{\mathrm{S},T}^{k+1}\underline{\boldsymbol{v}}_T\|_{U,T}.$$

Let us estimate $\mathfrak{T}_1(T)$. Recalling that $\boldsymbol{G}_T^k\circ\underline{\boldsymbol{I}}_T^k = \boldsymbol{\pi}_{\boldsymbol{\mathcal{P}},T}^k$ and using the approximation properties of this projector (cf. [15] and [19, Chapter 1] concerning the extension to non-star-shaped elements), it is readily inferred for the first factor

$$\mu_T^{1/2}h_T^{1/2}\|\boldsymbol{\nabla}\boldsymbol{w} - \boldsymbol{G}_T^k\underline{\boldsymbol{I}}_T^k\boldsymbol{w}\|_{\boldsymbol{L}^2(\partial T;\mathbb{R}^{d\times d})} \lesssim \mu_T^{1/2}h_T^{r+1}|\boldsymbol{w}|_{\boldsymbol{H}^{r+2}(T;\mathbb{R}^d)}.$$

The estimate of the second factor depends on the regime. If $C_{\mathrm{f},T} < 1$, using (15) we write

$$\frac{\mu_T}{h_T}\sum_{F\in\mathcal{F}_T}\|\boldsymbol{v}_F - \boldsymbol{v}_T\|^2_{\boldsymbol{L}^2(F;\mathbb{R}^d)} \lesssim \mu_T\|\underline{\boldsymbol{v}}_T\|^2_{\mathrm{S},T} = \mu_T\min(1,C_{\mathrm{f},T}^{-1})\|\underline{\boldsymbol{v}}_T\|^2_{\mathrm{S},T}, \tag{40}$$

where the conclusion follows observing that $1 = \min(1, C_{\mathrm{f},T}^{-1})$. If, on the other hand, $C_{\mathrm{f},T} \ge 1$ (which implies, in particular, $\nu_T > 0$), we insert $\pm\boldsymbol{P}_{\mathrm{D},T}^k\underline{\boldsymbol{v}}_T$ into the norm and use triangle and discrete trace inequalities to write

$$\begin{aligned}&\frac{\mu_T}{h_T}\sum_{F\in\mathcal{F}_T}\|\boldsymbol{v}_F - \boldsymbol{v}_T\|^2_{\boldsymbol{L}^2(F;\mathbb{R}^d)}\\ &\quad\lesssim \nu_T C_{\mathrm{f},T}^{-1}\left(h_T\sum_{F\in\mathcal{F}_T}\|\boldsymbol{v}_F - \boldsymbol{P}_{\mathrm{D},T}^k\underline{\boldsymbol{v}}_T\|^2_{\boldsymbol{L}^2(F;\mathbb{R}^d)} + \|\boldsymbol{v}_T - \boldsymbol{P}_{\mathrm{D},T}^k\underline{\boldsymbol{v}}_T\|^2_{\boldsymbol{L}^2(T;\mathbb{R}^d)}\right)\end{aligned}$$

$$\lesssim \nu_T C_{\mathrm{f},T}^{-1}\Bigg(h_T \sum_{F\in\mathcal{F}_T\cap\mathcal{F}_h^{\mathrm{b}}} \|\boldsymbol{v}_F - \boldsymbol{P}_{\mathrm{D},T}^k \underline{\boldsymbol{v}}_T\|_{\boldsymbol{L}^2(F;\mathbb{R}^d)}^2 + \|\underline{\boldsymbol{v}}_T - \underline{\boldsymbol{I}}_T^k \boldsymbol{P}_{\mathrm{D},T}^k \underline{\boldsymbol{v}}_T\|_{\boldsymbol{U},T}^2\Bigg)$$

where we have additionally used the definition (4) of $C_{\mathrm{f},T}$ in the first inequality, and continued invoking the definition of $\|\cdot\|_{\boldsymbol{U},T}$ (see (6)–(7)) to bound the element term and the non-boundary face terms in the second line by $\|\underline{\boldsymbol{v}}_T - \underline{\boldsymbol{I}}_T^k \boldsymbol{P}_{\mathrm{D},T}^k \underline{\boldsymbol{v}}_T\|_{\boldsymbol{U},T}^2$. For all $F \in \mathcal{F}_T \cap \mathcal{F}_h^{\mathrm{b}}$, we have $\boldsymbol{v}_F = \boldsymbol{0}$ by definition of $\underline{\boldsymbol{U}}_{h,0}^k$ and, using discrete trace inequalities and the mesh regularity to write $\mathrm{card}(\mathcal{F}_T) \lesssim 1$, we infer that

$$\begin{aligned}\frac{\mu_T}{h_T}\sum_{F\in\mathcal{F}_T} \|\boldsymbol{v}_F - \boldsymbol{v}_T\|_{\boldsymbol{L}^2(F;\mathbb{R}^d)}^2 &\lesssim \nu_T C_{\mathrm{f},T}^{-1}\left(\|\boldsymbol{P}_{\mathrm{D},T}^k \underline{\boldsymbol{v}}_T\|_{\boldsymbol{L}^2(T;\mathbb{R}^d)}^2 + \|\underline{\boldsymbol{v}}_T - \underline{\boldsymbol{I}}_T^k \boldsymbol{P}_{\mathrm{D},T}^k \underline{\boldsymbol{v}}_T\|_{\boldsymbol{U},T}^2\right)\\ &\lesssim \nu_T C_{\mathrm{f},T}^{-1} \|\underline{\boldsymbol{v}}_T\|_{\mathrm{D},T}^2,\end{aligned}$$

where the last passage follows recalling the definitions (28) of the $\|\cdot\|_{\mathrm{D},T}$-norm, (25) of $\widetilde{\boldsymbol{P}}_{\mathrm{D},T}^k$ (which is equal to $\boldsymbol{P}_{\mathrm{D},T}^k$ since $C_{\mathrm{f},T} \geq 1$), and observing that $1 = \min(1, C_{\mathrm{f},T})$. Hence, further observing that $C_{\mathrm{f},T}^{-1} = \min(1, C_{\mathrm{f},T}^{-1})$, we can go on writing

$$\frac{\mu_T}{h_T}\sum_{F\in\mathcal{F}_T} \|\boldsymbol{v}_F - \boldsymbol{v}_T\|_{\boldsymbol{L}^2(F;\mathbb{R}^d)}^2 \lesssim \nu_T \min(1, C_{\mathrm{f},T}^{-1}) \|\underline{\boldsymbol{v}}_T\|_{\mathrm{D},T}^2. \tag{41}$$

Gathering (40) and (41), we arrive at

$$\mathfrak{T}_1(T) \lesssim \mu_T^{1/2} \min(1, C_{\mathrm{f},T}^{-1})^{1/2} h_T^{r+1} |\boldsymbol{w}|_{\boldsymbol{H}^{r+2}(T;\mathbb{R}^d)} \left(\mu_T \|\underline{\boldsymbol{v}}_T\|_{\mathrm{S},T}^2 + \nu_T \|\underline{\boldsymbol{v}}_T\|_{\mathrm{D},T}^2\right)^{1/2}. \tag{42}$$

Moving to $\mathfrak{T}_2(T)$, using the $\|\cdot\|_{\boldsymbol{U},T}$-boundedness (8) of $\underline{\boldsymbol{I}}_T^k$ followed by the approximation properties of $\boldsymbol{P}_{\mathrm{S},T}^{k+1} \circ \underline{\boldsymbol{I}}_T^k$ (consequence, for each of its components, of [19, Eq. (2.14) and Theorem 1.48]), we have

$$\|\underline{\boldsymbol{I}}_T^k(\boldsymbol{w} - \boldsymbol{P}_{\mathrm{S},T}^{k+1} \underline{\boldsymbol{I}}_T^k \underline{\boldsymbol{w}})\|_{\boldsymbol{U},T} \lesssim \|\boldsymbol{w} - \boldsymbol{P}_{\mathrm{S},T}^{k+1} \underline{\boldsymbol{I}}_T^k \underline{\boldsymbol{w}}\|_{\boldsymbol{L}^2(T;\mathbb{R}^d)} + h_T |\boldsymbol{w} - \boldsymbol{P}_{\mathrm{S},T}^{k+1} \underline{\boldsymbol{I}}_T^k \underline{\boldsymbol{w}}|_{\boldsymbol{H}^1(T;\mathbb{R}^d)} \lesssim h_T^{r+2} |\boldsymbol{w}|_{\boldsymbol{H}^{r+2}(T;\mathbb{R}^d)}.$$

Plugging this estimate into the definition of $\mathfrak{T}_2(T)$ and recalling the definition (13) of $\|\cdot\|_{\mathrm{S},T}$, we get

$$\mathfrak{T}_2(T) \lesssim \mu_T^{1/2} \min(1, C_{\mathrm{f},T}^{-1})^{1/2} h_T^{r+1} |\boldsymbol{w}|_{\boldsymbol{H}^{r+2}(T;\mathbb{R}^d)}\, \mu_T^{1/2} \|\underline{\boldsymbol{v}}_T\|_{\mathrm{S},T}. \tag{43}$$

Using (42) and (43) to estimate the right-hand side of (39), we obtain

$$\begin{aligned}\mathcal{E}_{\mathrm{S},h}^k(\boldsymbol{w}; \underline{\boldsymbol{v}}_h) &\lesssim \sum_{T\in\mathcal{T}_h} \mu_T^{1/2} \min(1, C_{\mathrm{f},T}^{-1})^{1/2} h_T^{r+1} |\boldsymbol{w}|_{\boldsymbol{H}^{r+2}(T;\mathbb{R}^d)} \left(\mu_T \|\underline{\boldsymbol{v}}_T\|_{\mathrm{S},T}^2 + \nu_T \|\underline{\boldsymbol{v}}_T\|_{\mathrm{D},T}^2\right)^{1/2}\\ &\leq \left(\sum_{T\in\mathcal{T}_h} \mu_T \min(1, C_{\mathrm{f},T}^{-1}) h_T^{2(r+1)} |\boldsymbol{w}|_{\boldsymbol{H}^{r+2}(T;\mathbb{R}^d)}^2\right)^{1/2} \|\underline{\boldsymbol{v}}_h\|_{\mu,\nu,h},\end{aligned}$$

where the conclusion follows using a discrete Cauchy–Schwarz inequality on the sum over $T \in \mathcal{T}_h$ along with the definition (34) of $\|\cdot\|_{\mu,\nu,h}$. Dividing by $\|\underline{\boldsymbol{v}}_h\|_{\mu,\nu,h}$ and passing to the supremum concludes the proof of (38). □

5.2.2 Consistency of the Darcy bilinear form

Lemma 11 (Consistency of the Darcy bilinear form)**.** *Given $\boldsymbol{w} \in \boldsymbol{H}^1(\Omega;\mathbb{R}^d)$, let the Darcy consistency error linear form $\mathcal{E}_{\mathrm{D},h}^k(\boldsymbol{w};\cdot) : \underline{\boldsymbol{U}}_h^k \to \mathbb{R}$ be such that, for all $\underline{\boldsymbol{v}}_h \in \underline{\boldsymbol{U}}_h^k$,*

$$\mathcal{E}_{\mathrm{D},h}^k(\boldsymbol{w};\underline{\boldsymbol{v}}_h) \coloneqq \sum_{T\in\mathcal{T}_h}\int_T \nu_T\boldsymbol{w}\cdot\widetilde{\boldsymbol{P}}_{\mathrm{D},T}^k\underline{\boldsymbol{v}}_T - a_{\nu,h}(\underline{\boldsymbol{I}}_h^k\boldsymbol{w},\underline{\boldsymbol{v}}_h). \tag{44}$$

Then, further assuming $\boldsymbol{w} \in \boldsymbol{H}^{r+1}(\mathcal{T}_h;\mathbb{R}^d)$ for some $r \in \{0,\dots,k\}$, it holds

$$\|\mathcal{E}_{\mathrm{D},h}^k(\boldsymbol{w};\cdot)\|_{\mu,\nu,h,*} \lesssim \left(\sum_{T\in\mathcal{T}_h}\nu_T\min(1,C_{\mathrm{f},T})h_T^{2(r+1)}|\boldsymbol{w}|^2_{\boldsymbol{H}^{r+1}(T;\mathbb{R}^d)}\right)^{1/2}. \tag{45}$$

Proof. Let $\underline{\boldsymbol{v}}_h \in \underline{\boldsymbol{U}}_{h,0}^k \setminus \{\underline{\boldsymbol{0}}\}$. Expanding $a_{\nu,h}$ according to its definition (26), we get

$$\mathcal{E}_{\mathrm{D},h}^k(\boldsymbol{w};\underline{\boldsymbol{v}}_h) = \sum_{T\in\mathcal{T}_h}\left[\mathfrak{T}_1(T)+\mathfrak{T}_2(T)\right], \tag{46}$$

with

$$\begin{aligned}
\mathfrak{T}_1(T) &\coloneqq \int_T \nu_T(\boldsymbol{w}-\widetilde{\boldsymbol{P}}_{\mathrm{D},T}^k\underline{\boldsymbol{I}}_T^k\boldsymbol{w})\cdot\widetilde{\boldsymbol{P}}_{\mathrm{D},T}^k\underline{\boldsymbol{v}}_T,\\
\mathfrak{T}_2(T) &\coloneqq -\nu_T\min(1,C_{\mathrm{f},T})(\underline{\boldsymbol{I}}_T^k(\boldsymbol{w}-\boldsymbol{P}_{\mathrm{D},T}^k\underline{\boldsymbol{I}}_T^k\boldsymbol{w}),\underline{\boldsymbol{v}}_T-\underline{\boldsymbol{I}}_T^k\boldsymbol{P}_{\mathrm{D},T}^k\underline{\boldsymbol{v}}_T)_{U,T}.
\end{aligned}$$

The estimate of $\mathfrak{T}_1(T)$ depends on the regime. Let us start with the case $C_{\mathrm{f},T} \geq 1$. Recalling (25) to replace $\widetilde{\boldsymbol{P}}_{\mathrm{D},T}^k$ with $\boldsymbol{P}_{\mathrm{D},T}^k$ and applying a Cauchy–Schwarz inequality, we get

$$\begin{aligned}
|\mathfrak{T}_1(T)| &\lesssim \nu_T\|\boldsymbol{w}-\boldsymbol{P}_{\mathrm{D},T}^k\underline{\boldsymbol{I}}_T^k\boldsymbol{w}\|_{\boldsymbol{L}^2(T;\mathbb{R}^d)}\|\boldsymbol{P}_{\mathrm{D},T}^k\underline{\boldsymbol{v}}_T\|_{\boldsymbol{L}^2(T;\mathbb{R}^d)}\\
&\lesssim \nu_T^{1/2}\min(1,C_{\mathrm{f},T})^{1/2}h_T^{r+1}|\boldsymbol{w}|_{\boldsymbol{H}^{r+1}(T;\mathbb{R}^d)}\,\nu_T^{1/2}\|\underline{\boldsymbol{v}}_T\|_{\mathrm{D},T},
\end{aligned}$$

where, to pass to the second line, we have used the approximation properties (22) of $\boldsymbol{P}_{\mathrm{D},T}^k\circ\underline{\boldsymbol{I}}_T^k$ with $m=0$, the definition (28) of the $\|\cdot\|_{\mathrm{D},T}$-norm, and observed that $1=\min(1,C_{\mathrm{f},T})$.

Let us now consider the case $C_{\mathrm{f},T} < 1$. Recalling that $\widetilde{\boldsymbol{P}}_{\mathrm{D},T}^k\underline{\boldsymbol{I}}_T^k\boldsymbol{w} = \boldsymbol{\pi}_{\mathcal{P},T}^k\boldsymbol{w}$ in this case, we can write $\mathfrak{T}_1(T) = \int_T \nu_T(\boldsymbol{w}-\boldsymbol{\pi}_{\mathcal{P},T}^k\boldsymbol{w})\cdot(\boldsymbol{v}_T-\boldsymbol{\pi}_{\mathcal{P},T}^0\boldsymbol{v}_T)$ and, using Cauchy–Schwarz inequalities, continue with

$$|\mathfrak{T}_1(T)| \leq \nu_T\|\boldsymbol{w}-\boldsymbol{\pi}_{\mathcal{P},T}^k\boldsymbol{w}\|_{\boldsymbol{L}^2(T;\mathbb{R}^d)}\|\boldsymbol{v}_T-\boldsymbol{\pi}_{\mathcal{P},T}^0\boldsymbol{v}_T\|_{\boldsymbol{L}^2(T;\mathbb{R}^d)}. \tag{47}$$

Using the approximation properties of $\boldsymbol{\pi}_{\mathcal{P},T}^k$, it is readily inferred that the first factor is $\lesssim h_T^{r+1}|\boldsymbol{w}|_{\boldsymbol{H}^{r+1}(T;\mathbb{R}^d)}$. To estimate the last factor, we use a Poincaré–Wirtinger inequality to write $\|\boldsymbol{v}_T-\boldsymbol{\pi}_{\mathcal{P},T}^0\boldsymbol{v}_T\|_{\boldsymbol{L}^2(T;\mathbb{R}^d)} \lesssim h_T\|\boldsymbol{\nabla}\boldsymbol{v}_T\|_{\boldsymbol{L}^2(T;\mathbb{R}^{d\times d})} \lesssim h_T\|\underline{\boldsymbol{v}}_T\|_{\mathrm{S},T}$, where the conclusion follows from (15). Plugging the above estimates into (47), we can go on writing

$$\begin{aligned}
|\mathfrak{T}_1(T)| &\lesssim \nu_T^{1/2}h_T^{r+1}|\boldsymbol{w}|_{\boldsymbol{H}^{r+1}(T;\mathbb{R}^d)}\,\nu_T^{1/2}h_T\|\underline{\boldsymbol{v}}_T\|_{\mathrm{S},T}\\
&= \nu_T^{1/2}h_T^{r+1}|\boldsymbol{w}|_{\boldsymbol{H}^{r+1}(T;\mathbb{R}^d)}\,\mu_T^{1/2}C_{\mathrm{f},T}^{1/2}\|\underline{\boldsymbol{v}}_T\|_{\mathrm{S},T},\\
&= \nu_T^{1/2}\min(1,C_{\mathrm{f},T})^{1/2}h_T^{r+1}|\boldsymbol{w}|_{\boldsymbol{H}^{r+1}(T;\mathbb{R}^d)}\,\mu_T^{1/2}\|\underline{\boldsymbol{v}}_T\|_{\mathrm{S},T},
\end{aligned}$$

where we have used the definition (4) of $C_{\mathrm{f},T}$ to pass to the second line and, after rearranging the factors, the fact that $C_{\mathrm{f},T} = \min(1, C_{\mathrm{f},T})$ to conclude. Gathering the above estimates, we thus have

$$|\mathfrak{T}_1(T)| \lesssim \nu_T^{1/2} \min(1, C_{\mathrm{f},T})^{1/2} h_T^{r+1} |\boldsymbol{w}|_{\boldsymbol{H}^{r+1}(T;\mathbb{R}^d)} \left(\mu_T \|\underline{\boldsymbol{v}}_T\|_{\mathrm{S},T}^2 + \nu_T \|\underline{\boldsymbol{v}}_T\|_{\mathrm{D},T}^2\right)^{1/2}. \tag{48}$$

To estimate $\mathfrak{T}_2(T)$, we use a Cauchy–Schwarz inequality to write

$$\begin{aligned}
&|\mathfrak{T}_2(T)| \\
&\quad\le \nu_T^{1/2} \min(1, C_{\mathrm{f},T})^{1/2} \|\underline{\boldsymbol{I}}_T^k(\boldsymbol{w} - \boldsymbol{P}_{\mathrm{D},T}^k \underline{\boldsymbol{I}}_T^k \boldsymbol{w})\|_{\boldsymbol{U},T}\ \nu_T^{1/2} \min(1, C_{\mathrm{f},T})^{1/2} \|\underline{\boldsymbol{v}}_T - \underline{\boldsymbol{I}}_T^k \boldsymbol{P}_{\mathrm{D},T}^k \underline{\boldsymbol{v}}_T\|_{\boldsymbol{U},T} \\
&\quad\lesssim \nu_T^{1/2} \min(1, C_{\mathrm{f},T})^{1/2} \left(\|\boldsymbol{w} - \boldsymbol{P}_{\mathrm{D},T}^k \underline{\boldsymbol{I}}_T^k \boldsymbol{w}\|_{\boldsymbol{L}^2(T;\mathbb{R}^d)} + h_T |\boldsymbol{w} - \boldsymbol{P}_{\mathrm{D},T}^k \underline{\boldsymbol{I}}_T^k \boldsymbol{w}|_{\boldsymbol{H}^1(T;\mathbb{R}^d)}\right)\ \nu_T^{1/2} \|\underline{\boldsymbol{v}}_T\|_{\mathrm{D},T} \\
&\quad\lesssim \nu_T^{1/2} \min(1, C_{\mathrm{f},T})^{1/2} h_T^{r+1} |\boldsymbol{w}|_{\boldsymbol{H}^{r+1}(T;\mathbb{R}^d)}\ \nu_T^{1/2} \|\underline{\boldsymbol{v}}_T\|_{\mathrm{D},T},
\end{aligned} \tag{49}$$

where we have used the $\|\cdot\|_{\boldsymbol{U},T}$-boundedness (8) of $\underline{\boldsymbol{I}}_T^k$ along with the definition (28) of the $\|\cdot\|_{\mathrm{D},T}$-norm in the second inequality and the approximation properties (22) of $\boldsymbol{P}_{\mathrm{D},T}^k \circ \underline{\boldsymbol{I}}_T^k$ with $m = 0$ and $m = 1$ to conclude. Plugging (48) and (49) into (46), using discrete Cauchy–Schwarz inequalities, dividing by $\|\underline{\boldsymbol{v}}_h\|_{\mu,\nu,h}$, and passing to the supremum, the conclusion follows. □

5.2.3 Consistency of the coupling bilinear form

The quantity estimated in the following lemma can be interpreted as an adjoint consistency error for the discrete divergence.

Lemma 12 (Consistency of the coupling bilinear form)**.** *Given $q \in H^1(\Omega)$, let the coupling consistency error linear form $\mathcal{E}_{\mathrm{c},h}^k(q;\cdot) : \underline{\boldsymbol{U}}_{h,0}^k \to \mathbb{R}$ be such that, for all $\underline{\boldsymbol{v}}_h \in \underline{\boldsymbol{U}}_{h,0}^k$,*

$$\mathcal{E}_{\mathrm{c},h}^k(q;\underline{\boldsymbol{v}}_h) \coloneqq \sum_{T\in\mathcal{T}_h} \int_T \boldsymbol{\nabla} q \cdot \widetilde{\boldsymbol{P}}_{\mathrm{D},T}^k \underline{\boldsymbol{v}}_T - b_h(\underline{\boldsymbol{v}}_h, \pi_{\mathcal{P},h}^k q). \tag{50}$$

Then, further assuming, for some $r \in \{0,\dots,k\}$, $q \in H^{r+1+\langle C_{\mathrm{f},T}\ge 1\rangle}(T)$ for all $T \in \mathcal{T}_h$, it holds

$$\begin{aligned}
&\|\mathcal{E}_{\mathrm{c},h}^k(q;\cdot)\|_{\mu,\nu,h,*} \\
&\qquad\lesssim \left[\sum_{T\in\mathcal{T}_h} \left(\mu_T^{-1}\langle C_{\mathrm{f},T} < 1\rangle h_T^{2(r+1)} |q|_{H^{r+1}(T)}^2 + \nu_T^{-1}\langle C_{\mathrm{f},T} \ge 1\rangle h_T^{2(r+1)} |q|_{H^{r+2}(T)}^2\right)\right]^{1/2},
\end{aligned} \tag{51}$$

where $\nu_T^{-1}\langle C_{\mathrm{f},T} \ge 1\rangle \coloneqq 0$ if $\nu_T = 0$ as in Theorem 7.

Proof. Let $\underline{\boldsymbol{v}}_h \in \underline{\boldsymbol{U}}_{h,0}^k \setminus \{\underline{\boldsymbol{0}}\}$. We start by noticing that, expanding the bilinear form b_h according to its definition (29),

$$\mathcal{E}_{\mathrm{c},h}^k(q;\underline{\boldsymbol{v}}_h) = \sum_{T\in\mathcal{T}_h} \left(\int_T \boldsymbol{\nabla} q \cdot \widetilde{\boldsymbol{P}}_{\mathrm{D},T}^k \underline{\boldsymbol{v}}_T + \int_T \pi_{\mathcal{P},T}^k q\ D_T^k \underline{\boldsymbol{v}}_T - \sum_{F\in\mathcal{F}_T} \omega_{TF} \int_F q\ (\boldsymbol{v}_F \cdot \boldsymbol{n}_F)\right), \tag{52}$$

where the insertion of the last term in parenthesis is made possible by the single-valuedness of $q\ (\boldsymbol{v}_F \cdot \boldsymbol{n}_F)$ at interfaces along with the fact that $\boldsymbol{v}_F \cdot \boldsymbol{n}_F = 0$ for all $F \in \mathcal{F}_h^{\mathrm{b}}$. Denote by $\mathfrak{T}(T)$ the

argument of the summation in (52). To estimate this quantity, we distinguish two cases based on the value of $C_{\mathrm{f},T}$.

If $C_{\mathrm{f},T} < 1$, $\widetilde{\boldsymbol{P}}^k_{\mathrm{D},T}\underline{\boldsymbol{v}}_T = \boldsymbol{v}_T$ by (25), so that

$$\mathfrak{T}(T) = \int_T \boldsymbol{\nabla} q \cdot \boldsymbol{v}_T + \int_T \pi^k_{\mathcal{P},T} q \; D^k_T \underline{\boldsymbol{v}}_T - \sum_{F\in\mathcal{F}_T} \omega_{TF} \int_F q \; (\boldsymbol{v}_F \cdot \boldsymbol{n}_F).$$

Thus, proceeding as in the derivation of [19, Eq. (8.41)], we get

$$\begin{aligned}\mathfrak{T}(T) &\lesssim h_T^{r+1} |q|_{H^{r+1}(T)} \left(\frac{1}{h_T}\sum_{F\in\mathcal{F}_T} \|\boldsymbol{v}_T - \boldsymbol{v}_F\|^2_{\boldsymbol{L}^2(F;\mathbb{R}^d)}\right)^{1/2} \\ &\lesssim \mu_T^{-1/2} \langle C_{\mathrm{f},T} < 1\rangle^{1/2} h_T^{r+1} |q|_{H^{r+1}(T)} \, \mu_T^{1/2} \|\underline{\boldsymbol{v}}_T\|_{\mathrm{S},T},\end{aligned} \tag{53}$$

where we have used (15) to conclude.

If $C_{\mathrm{f},T} \geq 1$, on the other hand, we have $\widetilde{\boldsymbol{P}}^k_{\mathrm{D},T} = \boldsymbol{P}^k_{\mathrm{D},T}$ (cf. (25)), so that

$$\mathfrak{T}(T) = \left(\int_T \boldsymbol{\nabla} q \cdot \boldsymbol{P}^k_{\mathrm{D},T}\underline{\boldsymbol{v}}_T + \int_T \pi^k_{\mathcal{P},T} q \; D^k_T \underline{\boldsymbol{v}}_T - \sum_{F\in\mathcal{F}_T} \omega_{TF} \int_F q \; (\boldsymbol{v}_F \cdot \boldsymbol{n}_F)\right).$$

Using the definition (19) of $\boldsymbol{P}^k_{\mathrm{D},T}$ to proceed as in [17, Theorem 11], we get

$$\mathfrak{T}(T) \lesssim h_T^{r+1} |q|_{H^{r+2}(T)} \, \|\underline{\boldsymbol{v}}_T\|_{\mathrm{D},T} \leq \nu_T^{-1/2} \langle C_{\mathrm{f},T} \geq 1\rangle^{1/2} h_T^{r+1} |q|_{H^{r+2}(T)} \, \nu_T^{1/2} \|\underline{\boldsymbol{v}}_T\|_{\mathrm{D},T}, \tag{54}$$

where we have additionally noticed that $C_{\mathrm{f},T} \geq 1$ implies $\nu_T > 0$.

To conclude, we plug (53) and (54) into (52), use a Cauchy–Schwarz inequality on the sum over $T \in \mathcal{T}_h$, recall the definition (34) of the $\|\cdot\|_{\mu,\nu,h}$-norm, and pass to the supremum after dividing by $\|\underline{\boldsymbol{v}}_h\|_{\mu,\nu,h}$. □

Remark 13 (Discretisation of the source term). The use of $\boldsymbol{P}^k_{\mathrm{D},T}$ in the discretisation of the source term when $C_{\mathrm{f},T} \geq 1$ (see (32) and (25)) is crucial to ensure that, in this case, the consistency error of the coupling bilinear form can be bounded above using the Darcy norm instead of the Stokes norm; compare (54) and (53). This bound is key to establishing an error estimate in h^{r+1} that remains robust in the Darcy limit.

5.2.4 Consistency of the forcing term linear form

The following lemma estimates the difference between the standard HHO right-hand side linear form and the one obtained, as in (2a), using $\widetilde{\boldsymbol{P}}^k_{\mathrm{D},T}\underline{\boldsymbol{v}}_T$ instead of $\boldsymbol{v}_T$ as a test function.

Lemma 14 (Consistency of the forcing term)**.** *For any $\boldsymbol{\varphi} \in \boldsymbol{L}^2(\Omega;\mathbb{R}^d)$, define the right-hand side consistency error linear form $\mathcal{E}^k_{\mathrm{rhs},h}(\boldsymbol{\varphi};\cdot) : \underline{\boldsymbol{U}}^k_h \to \mathbb{R}$ such that, for all $\underline{\boldsymbol{v}}_h \in \underline{\boldsymbol{U}}^k_h$,*

$$\mathcal{E}^k_{\mathrm{rhs},h}(\boldsymbol{\varphi};\underline{\boldsymbol{v}}_h) \coloneqq \sum_{T\in\mathcal{T}_h} \int_T \boldsymbol{\varphi} \cdot (\boldsymbol{v}_T - \widetilde{\boldsymbol{P}}^k_{\mathrm{D},T}\underline{\boldsymbol{v}}_T). \tag{55}$$

Further assuming $\boldsymbol{\varphi} \in \boldsymbol{H}^r(\mathcal{T}_h;\mathbb{R}^d)$ for some $r \in \{0,\dots,k\}$, it holds

$$\|\mathcal{E}^k_{\mathrm{rhs},h}(\boldsymbol{\varphi};\cdot)\|_{\mu,\nu,h,*} \lesssim \left(\sum_{T\in\mathcal{T}_h} \mu_T^{-1} \min(1, C_{\mathrm{f},T}^{-1}) h_T^{2(r+1)} |\boldsymbol{\varphi}|^2_{\boldsymbol{H}^r(T;\mathbb{R}^d)}\right)^{1/2}. \tag{56}$$

Proof. Denote by $\mathfrak{T}(T)$ the argument of the summation in (55). If $C_{\mathrm{f},T} < 1$, the definition (25) of $\widetilde{\boldsymbol{P}}^k_{\mathrm{D},T}$ yields $\mathfrak{T}(T) = 0$. Consider now the case $C_{\mathrm{f},T} \geq 1$ (which implies, in particular, $\nu_T > 0$). We first notice that, letting $\boldsymbol{\pi}^{k-1}_{\boldsymbol{\mathcal{P}},T}\boldsymbol{\varphi} \coloneqq \mathbf{0}$ if $k = 0$,

$$\|\boldsymbol{\varphi} - \boldsymbol{\pi}^{k-1}_{\boldsymbol{\mathcal{P}},T}\boldsymbol{\varphi}\|_{\boldsymbol{L}^2(T;\mathbb{R}^d)} \lesssim h_T^r |\boldsymbol{\varphi}|_{\boldsymbol{H}^r(T;\mathbb{R}^d)}, \tag{57}$$

where the result is trivial if $k = 0$ (which imposes $r = 0$) and otherwise follows from the approximation properties of $\boldsymbol{\pi}^{k-1}_{\boldsymbol{\mathcal{P}},T}$, see [19, Theorem 1.45]. Recalling that, for $C_{\mathrm{f},T} \geq 1$, we have $\widetilde{\boldsymbol{P}}^k_{\mathrm{D},T} = \boldsymbol{P}^k_{\mathrm{D},T}$ by (25) and invoking (20) (which trivially holds also for $k = 0$), we then write

$$\begin{aligned}
\mathfrak{T}(T) &= \int_T (\boldsymbol{\varphi} - \boldsymbol{\pi}^{k-1}_{\boldsymbol{\mathcal{P}},T}\boldsymbol{\varphi}) \cdot (\boldsymbol{v}_T - \boldsymbol{P}^k_{\mathrm{D},T}\underline{\boldsymbol{v}}_T) \\
&\leq \|\boldsymbol{\varphi} - \boldsymbol{\pi}^{k-1}_{\boldsymbol{\mathcal{P}},T}\boldsymbol{\varphi}\|_{\boldsymbol{L}^2(T;\mathbb{R}^d)} \|\boldsymbol{v}_T - \boldsymbol{P}^k_{\mathrm{D},T}\underline{\boldsymbol{v}}_T\|_{\boldsymbol{L}^2(T;\mathbb{R}^d)} \\
&\lesssim \mu_T^{-1/2} h_T^r |\boldsymbol{\varphi}|_{\boldsymbol{H}^r(T;\mathbb{R}^d)}\ h_T \mu_T^{1/2} h_T^{-1} \|\underline{\boldsymbol{v}}_T\|_{\mathrm{D},T} \\
&= \mu_T^{-1/2} h_T^{r+1} |\boldsymbol{\varphi}|_{\boldsymbol{H}^r(T;\mathbb{R}^d)}\ \nu_T^{1/2} \min(1, C_{\mathrm{f},T}^{-1})^{1/2} \|\underline{\boldsymbol{v}}_T\|_{\mathrm{D},T},
\end{aligned}$$

where we have used Cauchy–Schwarz inequalities in the first passage, the approximation properties (57) of the L^2-orthogonal projector for the first factor together with the definitions (7) and (28) of $\|\cdot\|_{U,T}$ and $\|\cdot\|_{\mathrm{D},T}$ to write $\|\boldsymbol{v}_T - \boldsymbol{P}^k_{\mathrm{D},T}\underline{\boldsymbol{v}}_T\|_{\boldsymbol{L}^2(T;\mathbb{R}^d)} \leq \|\underline{\boldsymbol{v}}_T - \underline{\boldsymbol{I}}^k_T \boldsymbol{P}^k_{\mathrm{D},T}\underline{\boldsymbol{v}}_T\|_{U,T} \leq \|\underline{\boldsymbol{v}}_T\|_{\mathrm{D},T}$ in the second passage, while the conclusion follows from the definition (4) of $C_{\mathrm{f},T}$ along with $C_{\mathrm{f},T}^{-1} = \min(1, C_{\mathrm{f},T}^{-1})$. Using the above estimate in (55), applying a Cauchy–Schwarz inequality on the sum over $T \in \mathcal{T}_h$, and recalling the definition (34) of $\|\cdot\|_{\mu,\nu,h}$, (56) follows. □

5.2.5 Proof of Theorem 7

Proof of Theorem 7. Since $a_{\mu,h} + a_{\nu,h}$ is 1-coercive and has norm 1 for the $\|\cdot\|_{\mu,\nu,h}$ norm, Lemma 6 and [19, Lemma A.11] show that $\mathcal{A}_h$ is γ-inf-sup stable for the norm in the left-hand side of (35). Hence, in the spirit of the third Strang lemma [16], this error estimate follows if we bound the consistency error by the bracketed term in the right-hand side. The consistency error for the scheme (32) is

$$\begin{aligned}
\mathcal{E}^k_h(\boldsymbol{u}, p; \underline{\boldsymbol{v}}_h) &\coloneqq \sum_{T\in\mathcal{T}_h} \int_T \boldsymbol{f} \cdot \widetilde{\boldsymbol{P}}^k_{\mathrm{D},T}\underline{\boldsymbol{v}}_T + \int_\Omega g q_h - \mathcal{A}_h((\underline{\boldsymbol{I}}^k_h \boldsymbol{u}, \pi^h_{\mathcal{P},k} p), (\underline{\boldsymbol{v}}_h, q_h)) \\
&= \sum_{T\in\mathcal{T}_h} \int_T \boldsymbol{\nabla}\cdot(\mu_T \boldsymbol{\nabla}\boldsymbol{u}) \cdot (\boldsymbol{v}_T - \widetilde{\boldsymbol{P}}^k_{\mathrm{D},T}\underline{\boldsymbol{v}}_T) - \sum_{T\in\mathcal{T}_h} \int_T \boldsymbol{\nabla}\cdot(\mu_T \boldsymbol{\nabla}\boldsymbol{u}) \cdot \boldsymbol{v}_T - a_{\mu,h}(\underline{\boldsymbol{I}}^k_h \boldsymbol{u}, \underline{\boldsymbol{v}}_h) \\
&\quad + \sum_{T\in\mathcal{T}_h} \int_T \nu_T \boldsymbol{u} \cdot \widetilde{\boldsymbol{P}}^k_{\mathrm{D},T}\underline{\boldsymbol{v}}_T - a_{\nu,h}(\underline{\boldsymbol{I}}^k_h \boldsymbol{u}, \underline{\boldsymbol{v}}_h) + \sum_{T\in\mathcal{T}_h} \int_T \boldsymbol{\nabla} p \cdot \widetilde{\boldsymbol{P}}^k_{\mathrm{D},T}\underline{\boldsymbol{v}}_T - b_h(\underline{\boldsymbol{v}}_h, \pi^k_{\mathcal{P},h} p) \\
&\quad + \cancel{\int_\Omega g q_h + b_h(\underline{\boldsymbol{I}}^k_h \boldsymbol{u}, q_h)} \\
&= \mathcal{E}^k_{\mathrm{rhs},h}(\boldsymbol{\nabla}\cdot(\mu\boldsymbol{\nabla}\boldsymbol{u}); \underline{\boldsymbol{v}}_h) + \mathcal{E}^k_{\mathrm{S},h}(\boldsymbol{u}; \underline{\boldsymbol{v}}_h) + \mathcal{E}^k_{\mathrm{D},h}(\boldsymbol{u}; \underline{\boldsymbol{v}}_h) + \mathcal{E}^k_{\mathrm{c},h}(p; \underline{\boldsymbol{v}}_h),
\end{aligned} \tag{58}$$

where we have we have replaced $\boldsymbol{f}$ with the left-hand side of (2a), expanded $\mathcal{A}_h$ according to its definition (33), and used (30) along with (2b) to cancel the last term in the first passage, and used the definitions of the consistency errors (55) with $\boldsymbol{\varphi} = \boldsymbol{\nabla}\cdot(\mu\boldsymbol{\nabla}\boldsymbol{u})$, (37) and (44) with $\boldsymbol{w} = \boldsymbol{u}$, and (50) with $q = p$ to conclude.

Using, respectively, (56) (further noticing that $|\boldsymbol{\nabla}\cdot(\mu_T\boldsymbol{\nabla}\boldsymbol{u})|_{\boldsymbol{H}^r(T;\mathbb{R}^d)} \lesssim \mu_T|\boldsymbol{u}|_{\boldsymbol{H}^{r+2}(T;\mathbb{R}^d)}$ for all $T \in \mathcal{T}_h$), (38), (45), and (51) to estimate the terms in the right-hand side of (58), the result follows. □

Acknowledgements

This research received support from the ANR "NEMESIS" (ANR-20-MRS2-0004) and the Australian Research Council's Discovery Projects funding scheme (DP210103092). The authors would also like to thank Ricardo Ruiz-Baier for sharing Gmsh geometry files at the source of the tests in Section 4.2.

References

[1] M. Alvarez, G. N. Gatica, and R. Ruiz-Baier. "A vorticity-based fully-mixed formulation for the 3D Brinkman-Darcy problem". In: *Comput. Methods Appl. Mech. Engrg.* 307 (2016), pp. 68–95. DOI: 10.1016/j.cma.2016.04.017.

[2] V. Anaya, G. N. Gatica, D. Mora, and R. Ruiz-Baier. "An augmented velocity-vorticity-pressure formulation for the Brinkman equations". In: *Internat. J. Numer. Methods Fluids* 79.3 (2015), pp. 109–137. DOI: 10.1002/fld.4041.

[3] D. Anderson and J. Droniou. "An arbitrary order scheme on generic meshes for miscible displacements in porous media". In: *SIAM J. Sci. Comput.* 40.4 (2018), B1020–B1054. DOI: 10.1137/17M1138807.

[4] R. Araya, C. Harder, A. H. Poza, and F. Valentin. "Multiscale hybrid-mixed method for the Stokes and Brinkman equations—the method". In: *Comput. Methods Appl. Mech. Engrg.* 324 (2017), pp. 29–53. DOI: 10.1016/j.cma.2017.05.027.

[5] D. Arnold. *Finite Element Exterior Calculus*. SIAM, 2018. DOI: 10.1137/1.9781611975543.

[6] C. Bernardi, F. Hecht, and F. Z. Nouri. "A new finite-element discretization of the Stokes problem coupled with the Darcy equations". In: *IMA J. Numer. Anal.* 30.1 (2010), pp. 61–93. DOI: 10.1093/imanum/drn054.

[7] D. Boffi, F. Brezzi, and M. Fortin. *Mixed finite element methods and applications*. Vol. 44. Springer Series in Computational Mathematics. Heidelberg: Springer, 2013, pp. xiv+685. DOI: 10.1007/978-3-642-36519-5.

[8] M. Bogovskiĭ. "Theory of cubature formulas and the application of functional analysis to problems of mathematical physics". In: vol. 149(1). Trudy Sem. S. L. Soboleva. Novosibirsk, Russia: Akad. Nauk SSSR Sibirsk. Otdel. Inst. Mat., 1980. Chap. Solutions of some problems of vector analysis associated with the operators div and grad, pp. 5–40.

[9] L. Botti and D. A. Di Pietro. "p-Multilevel preconditioners for HHO discretizations of the Stokes equations with static condensation". In: *Commun. Appl. Math. Comput.* 4.3 (2022), pp. 783–822. DOI: 10.1007/s42967-021-00142-5.

[10] L. Botti, D. A. Di Pietro, and J. Droniou. "A Hybrid High-Order discretisation of the Brinkman problem robust in the Darcy and Stokes limits". In: *Comput. Meth. Appl. Mech. Engrg.* 341 (2018), pp. 278–310. DOI: 10.1016/j.cma.2018.07.004.

[11] M. Botti, D. A. Di Pietro, and A. Guglielmana. "A low-order nonconforming method for linear elasticity on general meshes". In: *Comput. Meth. Appl. Mech. Engrg.* 354 (2019), pp. 96–118. DOI: 10.1016/j.cma.2019.05.031.

[12] E. Burman and P. Hansbo. "A unified stabilized method for Stokes' and Darcy's equations". In: *J. Comput. Appl. Math.* 198.1 (2007), pp. 35–51. DOI: 10.1016/j.cam.2005.11.022.

[13] E. Burman and P. Hansbo. "Stabilized Crouzeix-Raviart element for the Darcy-Stokes problem". In: *Numer. Methods Partial Differential Equations* 21.5 (2005), pp. 986–997. DOI: 10.1002/num.20076.

[14] E. Cáceres, G. N. Gatica, and F. A. Sequeira. "A mixed virtual element method for the Brinkman problem". In: *Math. Models Methods Appl. Sci.* 27.4 (2017), pp. 707–743. DOI: 10.1142/S0218202517500142.

[15] D. A. Di Pietro and J. Droniou. "A Hybrid High-Order method for Leray–Lions elliptic equations on general meshes". In: *Math. Comp.* 86.307 (2017), pp. 2159–2191. DOI: 10.1090/mcom/3180.

[16] D. A. Di Pietro and J. Droniou. "A third Strang lemma for schemes in fully discrete formulation". In: *Calcolo* 55.40 (2018). DOI: 10.1007/s10092-018-0282-3.

[17] D. A. Di Pietro and J. Droniou. "An arbitrary-order discrete de Rham complex on polyhedral meshes: Exactness, Poincaré inequalities, and consistency". In: *Found. Comput. Math.* (2021). DOI: 10.1007/s10208-021-09542-8.

[18] D. A. Di Pietro and J. Droniou. "An arbitrary-order method for magnetostatics on polyhedral meshes based on a discrete de Rham sequence". In: *J. Comput. Phys.* 429.109991 (2021). DOI: 10.1016/j.jcp.2020.109991.

[19] D. A. Di Pietro and J. Droniou. *The Hybrid High-Order method for polytopal meshes. Design, analysis, and applications*. Modeling, Simulation and Application 19. Springer International Publishing, 2020. DOI: 10.1007/978-3-030-37203-3.

[20] D. A. Di Pietro, J. Droniou, and F. Rapetti. "Fully discrete polynomial de Rham sequences of arbitrary degree on polygons and polyhedra". In: *Math. Models Methods Appl. Sci.* 30.9 (2020), pp. 1809–1855. DOI: 10.1142/S0218202520500372.

[21] D. A. Di Pietro and A. Ern. "A hybrid high-order locking-free method for linear elasticity on general meshes". In: *Comput. Meth. Appl. Mech. Engrg.* 283 (2015), pp. 1–21. DOI: 10.1016/j.cma.2014.09.009.

[22] D. A. Di Pietro and A. Ern. "Arbitrary-order mixed methods for heterogeneous anisotropic diffusion on general meshes". In: *IMA J. Numer. Anal.* 37.1 (2017), pp. 40–63. DOI: 10.1093/imanum/drw003.

[23] D. A. Di Pietro, A. Ern, and S. Lemaire. "An arbitrary-order and compact-stencil discretization of diffusion on general meshes based on local reconstruction operators". In: *Comput. Meth. Appl. Math.* 14.4 (2014), pp. 461–472. DOI: 10.1515/cmam-2014-0018.

[24] D. A. Di Pietro, A. Ern, A. Linke, and F. Schieweck. "A discontinuous skeletal method for the viscosity-dependent Stokes problem". In: *Comput. Meth. Appl. Mech. Engrg.* 306 (2016), pp. 175–195. DOI: 10.1016/j.cma.2016.03.033.

[25] R. G. Durán and M. A. Muschietti. "An explicit right inverse of the divergence operator which is continuous in weighted norms". In: *Studia Math.* 148.3 (2001), pp. 207–219. DOI: 10.4064/sm148-3-2.

[26] J. A. Evans and T. J. R. Hughes. "Isogeometric divergence-conforming B-splines for the Darcy-Stokes-Brinkman equations". In: *Math. Models Methods Appl. Sci.* 23.4 (2013), pp. 671–741. DOI: 10.1142/S0218202512500583.

[27] V. Girault and P.-A. Raviart. *Finite element methods for Navier-Stokes equations*. Vol. 5. Springer Series in Computational Mathematics. Theory and algorithms. Berlin: Springer-Verlag, 1986, pp. x+374.

[28] M. Juntunen and R. Stenberg. "Analysis of finite element methods for the Brinkman problem". In: *Calcolo* 47.3 (2010), pp. 129–147. DOI: 10.1007/s10092-009-0017-6.

[29] J. Könnö and R. Stenberg. "$H(\mathrm{div})$-conforming finite elements for the Brinkman problem". In: *Math. Models Methods Appl. Sci.* 21.11 (2011), pp. 2227–2248. DOI: 10.1142/S0218202511005726.

[30] K. A. Mardal, X.-C. Tai, and R. Winther. "A robust finite element method for Darcy-Stokes flow". In: *SIAM J. Numer. Anal.* 40.5 (2002), pp. 1605–1631. DOI: 10.1137/S0036142901383910.

[31] J.-C. Nédélec. "Mixed finite elements in $\mathbf{R}^3$". In: *Numer. Math.* 35.3 (1980), pp. 315–341. DOI: 10.1007/BF01396415.

[32] P. A. Raviart and J. M. Thomas. "A mixed finite element method for 2nd order elliptic problems". In: *Mathematical Aspects of the Finite Element Method*. Ed. by I. Galligani and E. Magenes. New York: Springer, 1977.

[33] V. A. Solonnikov. "L^p-estimates for solutions of the heat equation in a dihedral angle". In: *Rend. Mat. Appl.* 21 (2001), pp. 1–15.

[34] G. Vacca. "An H^1-conforming virtual element for Darcy and Brinkman equations". In: *Math. Models Methods Appl. Sci.* 28.1 (2018), pp. 159–194. DOI: 10.1142/S0218202518500057.